

## Small molecule SUMO inhibition for biomarker-informed B-cell lymphoma therapy

by Uta M. Demel, Matthias Wirth, Schayan Yousefian, Le Zhang, Konstandina Isaakidis, Judith Dönig, Marlitt Böger, Nikita Singh, Hazal Köse, Simon Haas, Stefan Müller, Markus Schick, and Ulrich Keller

Received: March 7, 2022.

Accepted: September 13, 2022.

*Citation: Uta M. Demel, Matthias Wirth, Schayan Yousefian, Le Zhang, Konstandina Isaakidis, Judith Dönig, Marlitt Böger, Nikita Singh, Hazal Köse, Simon Haas, Stefan Müller, Markus Schick, and Ulrich Keller. Small molecule SUMO inhibition for biomarker-informed B-cell lymphoma therapy. Haematologica. 2022 Sept 22. doi: 10.3324/haematol.2022.280995 [Epub ahead of print]*

### Publisher's Disclaimer.

E-publishing ahead of print is increasingly important for the rapid dissemination of science. Haematologica is, therefore, E-publishing PDF files of an early version of manuscripts that have completed a regular peer review and have been accepted for publication. E-publishing of this PDF file has been approved by the authors. After having E-published Ahead of Print, manuscripts will then undergo technical and English editing, typesetting, proof correction and be presented for the authors' final approval; the final version of the manuscript will then appear in a regular issue of the journal. All legal disclaimers that apply to the journal also pertain to this production process.

## ARTICLE

# Small molecule SUMO inhibition for biomarker-informed B-cell lymphoma therapy

Uta M. Demel<sup>1,2,3</sup>, Matthias Wirth<sup>1,2</sup>, Schayan Yousefian<sup>1,4,5</sup>, Le Zhang<sup>1,2</sup>, Konstandina Isaakidis<sup>1,2</sup>, Judith Dönig<sup>6</sup>, Marlitt Böger<sup>1,2</sup>, Nikita Singh<sup>1,2</sup>, Hazal Köse<sup>1,2</sup>, Simon Haas<sup>1,4,5,7,8,9</sup>, Stefan Müller<sup>6</sup>, Markus Schick<sup>1,2</sup> and Ulrich Keller<sup>1,2,7</sup>

<sup>1</sup>Department of Hematology, Oncology and Cancer Immunology, Campus Benjamin Franklin, Charité - Universitätsmedizin Berlin, corporate member of Freie Universität Berlin and Humboldt-Universität zu Berlin, 12203 Berlin, Germany

<sup>2</sup>Max-Delbrück-Center for Molecular Medicine, 13125 Berlin, Germany

<sup>3</sup>Clinician Scientist Program, Berlin Institute of Health (BIH), Berlin, Germany.

<sup>4</sup>Berlin Institute of Health (BIH) at Charité – Universitätsmedizin Berlin, 10117 Berlin, Germany

<sup>5</sup>Berlin Institute for Medical Systems Biology, Max Delbrück Center for Molecular Medicine in the Helmholtz Association, 10115 Berlin, Germany

<sup>6</sup>Institute of Biochemistry II, Goethe University Frankfurt, Medical School, 60590 Frankfurt, Germany

<sup>7</sup>German Cancer Consortium (DKTK), German Cancer Research Center (DKFZ), 69120 Heidelberg, Germany

<sup>8</sup>Heidelberg Institute for Stem Cell Technology and Experimental Medicine (HI-STEM gGmbH), 69120 Heidelberg, Germany

<sup>9</sup>Division of Stem Cells and Cancer, Deutsches Krebsforschungszentrum (DKFZ) and DKFZ-ZMBH Alliance, 69120 Heidelberg, Germany

Corresponding Author: Ulrich Keller, Department of Hematology, Oncology and Cancer Immunology, Campus Benjamin Franklin, Charité - Universitätsmedizin Berlin, Berlin, Germany, e-mail: ulrich.keller@charite.de

**Running title:** SUMO inhibition for MYC-dependent B-cell lymphoma

**Word count text:** 3292

**Word count abstract:** 146

**Figure count:** 4

**References:** 47

**Key words:** SUMO | MYC | B-cell lymphoma | immune activation

**Data sharing statement:** Sequencing data were uploaded to the European Nucleotide Archive and are publicly available via accession ID: PRJEB53800.

**Acknowledgments:** The authors would like to thank Millennium Pharmaceuticals, Inc., a wholly owned subsidiary of Takeda Pharmaceutical Company Limited, for providing ML-093 and subasumstat/Tak-981. This work was supported by Deutsche Forschungsgemeinschaft (DFG, SFB824/C3 and SFB1335/P3 to U.K.; grant KE 222/10-1 to U.K. S.M., DFG grants MU 1764/7-1 (#494535244) and MU 1764/7-1 to S.M.), Deutsche Krebshilfe (grants 70114425 and 70114724 to U.K., grant 70114823 to S.M.), Stiftung Charité (to U.K.), and Wilhelm-Sander Foundation (2017.048.2 to U.K.). U.D. is participant in the BIH-Charité Junior Clinician Scientist program funded by the Charité - Universitätsmedizin Berlin and the Berlin Institute of Health.

**Conflict of Interest:** U.K. received reimbursement for advisory board function, speaker honorary and travel support from Takeda for content unrelated to this manuscript. The other authors report no conflict of interest.

**Author Contributions:** Conception and design of the study: U.D., M.W., M.S., U.K.; Acquisition of data and/or analysis and interpretation of data: U.D., M.W., S.Y., L.Z., K.I., J.D., M.B., N.S., H.K., S.H., S.M., M.S., U.K.; Drafting of the manuscript: U.D., M.W., M.S., U.K.; All authors revised the manuscript for important intellectual content and approved the final version submitted for publication.

**ABSTRACT**

Aberrant activity of the SUMOylation pathway has been associated with MYC overexpression and poor prognosis in aggressive B-cell lymphoma (BCL) and other malignancies. Recently developed small molecule inhibitors of SUMOylation (SUMO $\text{i}$ ) target the heterodimeric E1 SUMO activation complex (SAE1/UBA2). Here, we report that activated MYC signaling is an actionable molecular vulnerability *in vitro* and in a pre-clinical murine *in vivo* model of MYC-driven BCL. While SUMO $\text{i}$  conferred direct effects on MYC-driven lymphoma cells, SUMO inhibition also resulted in substantial remodeling of various subsets of the innate and specific immunity *in vivo*. Specifically, SUMO $\text{i}$  increased the number of memory B-cells as well as cytotoxic and memory T-cells, subsets that are attributed a key role within a coordinated anti-tumor immune response. In summary, our data constitute pharmacologic SUMO $\text{i}$  as a powerful therapy in a subset of B-cell lymphomas causing massive remodeling of the normal B-cell and T-cell compartment.

## INTRODUCTION

The myelocytomatosis oncogene *MYC* is deregulated in almost half of all human cancers by chromosomal amplification, translocation or mutations in signaling pathways that regulate *MYC* expression<sup>1-3</sup>. *MYC* belongs to a family of basic helix-loop-helix leucin zipper DNA binding proteins that function as a transcription factor controlling multiple biological processes including cell proliferation, differentiation, apoptosis and metabolism<sup>1</sup>. Control of gene transcription is a well-established function of *MYC*, while *MYC* also interferes with translation and protein turnover<sup>4, 5</sup>. Genetic and epigenetic dysregulation of *MYC* expression accelerates cell proliferation and drives malignant transformation. So far, there are no effective therapies specifically targeting *MYC* signaling that have been established for clinical use. Uncontrolled cell growth in response to *MYC* overexpression creates dependencies on *MYC*-driven pathways to maintain the tumor phenotype<sup>6</sup>. Therefore, the idea of targeting these cellular processes has been developed within the concept of “synthetic lethal interactions”<sup>7, 8</sup>.

SUMOylation is a post-translational protein modification that controls localization, function and half-life of target proteins<sup>9, 10</sup>. It emerged as a crucial regulatory mechanism for fundamental cellular processes like chromatin organization, transcription and cell proliferation<sup>11</sup>. The conjugation of SUMO (SUMO1, SUMO2 or SUMO3) to its substrates is controlled by a multi-step cascade involving the E1 SUMO-activating enzyme SAE1/UBA2, the E2 SUMO-conjugating enzyme UBC9, and various E3 SUMO ligases<sup>12</sup>. SUMOylation is a fully reversible protein modification. Deconjugation of SUMO from its substrates is catalyzed by SUMO-specific proteases (or deconjugases) of the SENP (sentrin-specific protease) family<sup>13</sup>. Disruption of this well-controlled balance contributes to tumor development and progression<sup>14, 15</sup>. Of note, dysregulation of oncogenes such as *MYC* activates SUMOylation and hyperSUMOylation often correlates with poor prognosis in cancer<sup>16, 17</sup>. However, while activated SUMOylation is a key feature of aggressive cancers, the impact of activated SUMOylation on tumor biology is multifaceted<sup>9, 10</sup>. Besides its effect on cancer biology itself, SUMOylation restrains anti-tumor immunity by repression of

interferon signaling<sup>18-20</sup>. Since SUMOylation is activated in cancer cells with high MYC levels, targeting MYC-induced SUMOylation as a therapeutic vulnerability seems highly attractive<sup>7, 21-23</sup>. A selective small molecule inhibitor of SUMOylation that blocks activation of SUMO by the E1 activation enzyme was developed as ML-792 and further refined as ML-093. The clinically applicable form subasumstat (formerly TAK-981)<sup>24, 25</sup> is currently investigated in clinical trials (NCT03648372, NCT04074330, NCT04381650).

Here, we investigated SUMOylation as a MYC-induced molecular vulnerability in aggressive BCL. We uncovered that activated MYC signaling confers susceptibility to pharmacologic SUMO inhibition (SUMOi) in MYC-driven BCL. Next to direct effects on MYC-driven lymphoma, SUMOi challenge resulted in pronounced remodeling of the immune cell landscape.

## METHODS

**Chemicals.** SUMOi (ML-093 and Tak-981, as specified in the figure legends) was either purchased from MedChemExpress or provided by Millennium Pharmaceuticals, Inc., a wholly owned subsidiary of Takeda Pharmaceutical Company Limited. SUMOi doses and treatment durations are indicated in the figure legends.

**Cell Culture.** Human DLBCL cell lines were kept in RPMI-1640 (U-2932, NU-DHL-1, SU-DHL-4/5/6/8, DB and Toledo), IMDM (Oci-Ly1) or alpha-MEM (Oci-Ly19) medium supplemented with 10-20% FCS, 1% Penicillin Streptomycin and 2mM L-Glutamine (Thermo Scientific).

**Flow cytometry.** Cells were washed in HF2 buffer (ddH<sub>2</sub>O, 2 % FCS, 1 % Penicillin Streptomycin, 1 % Hepes, 10 % HBSS) and stained on ice for 30 min in HF2 (a list of all antibodies is provided in the supplementary material). After washing in HF2 cells were either resuspended in HF2 containing DAPI or PI for FACS analysis, stained with the respective antibody combination or fixed with BD Cytofix/Cytoperm for intracellular staining. Data were acquired on Beckman Coulter CytoFLEX S.

**Immunoblot analysis.** Protein extracts were prepared by solving cell pellets in lysis buffer (150mM NaCl, 1% NP-40 oder IGEPAL, 0.5% sodium deoxycholate, 0.1% SDS, 50 mM Tris) supplemented with NaF, PMSF and NaVO<sub>4</sub> followed by sonification. Protein lysates were fractioned on SDS PAGE gels, transferred to PVDF Transfer Membran (Thermo Scientific) and incubated with primary antibodies overnight. MYC antibody was obtained by Cell signaling (9402S) and β-tubulin by DSHB (E7). HRP-conjugated secondary antibodies allowed signal detection via enhanced chemiluminescence (ECL) reagents (Millipore).

**Cell viability assay.** 20k cells per well were seeded and treatments were administered as indicated. After 24, 48 and 72h incubation, CellTiterGlo (Promega, G7572) was added and luminescence was measured and normalized to DMSO control.

**Mice.** Wt mice (CD45.1, C57Bl/6J) were obtained from the Jackson Laboratory. Mice were examined twice a week. All animal experiments were performed in accordance to local authorities (Regierung von Oberbayern, Munich, Germany).

**Transplantation and *in vivo* treatment of mice.** 1x10<sup>6</sup> *Eμ-myc* cells (CD45.2) were transplanted i.v. into C57Bl/6J wt mice. SUMOi or carrier treatment to tumor or wt mice was administered i.v., doses and treatment duration are indicated in the figure legend.

**RNA-Seq and processing of gene expression data.** RNA samples were processed and sequenced (paired end, 150bp/read) by Novogene (Cambridge, UK) on a HiSeq2500 Illumina device with a read depth of >20M reads. Subsequent quality control, data processing and analysis were performed as described<sup>26</sup>. Sequencing data were uploaded to the European Nucleotide Archive and are available via accession ID: PRJEB53800. Further processing of transcriptomic data including gene set enrichment analysis is described in Supplemental Methods.

**Single Cell RNA-seq analysis.** A detailed description of the methods is provided in Supplemental Methods.

**Statistical analysis.** Statistical analyses were performed using GraphPad Prism (GraphPad Software). The error bars shown in the figures represent the standard deviation (SD), unless

specified otherwise. A *P*-value lower than 0.05 was generally considered significant and all exact *P*-values and tests are indicated in the figures.

**Study approval.** All animal experiments were performed in accordance to local authorities (Regierung Oberbayern, Munich, Germany and LAGeSo Berlin, Germany).

## RESULTS

### Activated MYC signaling confers susceptibility to small molecule SUMO inhibition in DLBCL cell lines

Activation of the oncprotein MYC is associated with a hyperSUMOylated phenotype in diffuse large B-cell lymphoma (DLBCL) (Fig. 1A, B) and both MYC overexpression and enhanced SUMO pathway activity are correlated with adverse clinical outcome (Fig. 1SA-C).

Given the role of MYC in DLBCL, we investigated the sensitivity of DLBCL cell lines to pharmacological SUMO inhibition<sup>24, 25</sup>. Three out of 10 cell lines (SU-DHL-8, SU-DHL-5 and Oci-Ly19) were responsive to SUMOi with viabilities below 25% at the highest SUMOi concentration (2000nM) (Fig. 1C, subasumstat; Fig. S1D, ML-093). Importantly, the broad range of response from exquisite sensitivity (SU-DHL-8, SU-DHL5, Oci-Ly19) to very minor response/non-response in the remainder of DLBCL cell lines revealed that the complex genetic and non-genetic background and dependencies of DLBCL likely define the response to SUMOi.

To systematically identify potential biomarkers predictive for SUMOi sensitivity, we ranked the cell lines according to their subasumstat GI50 values and classified the lower third of the panel as SUMOi-responders, and the remaining two-third constituting the SUMOi low sensitivity/non-responder subset. Gene set enrichment analysis identified the SUMO core pathway to be enhanced as well as various SUMOylation signatures to be enriched in the SUMOi-responsive cell lines (Fig. 1D; Fig. S1E), whereas baseline growth characteristics and doubling time were not directly correlated with sensitivity to SUMOi (Fig. S1F, G). Moreover, sensitivity to SUMOi treatment was associated with activated MYC signaling and MYC hallmark gene sets scored among the top enriched gene sets in SUMOi-responsive cell

lines (Fig. 1D, E; Fig. S1H). Of note, the SU-DHL-8 and Oci-Ly19 cell lines, which had the highest activity of MYC signaling (SU-DHL-8 also harbors an *IG::MYC* translocation), were among the most sensitive cell line within the investigated panel (Fig. 1C; Fig. S1D, G). We thus concluded that activated MYC signaling is an actionable molecular vulnerability and would predict response to SUMO<sub>i</sub>. To experimentally validate these findings and prove a causal relationship, we ectopically expressed MYC in the human Oci-Ly1 cell line, classified as a non-responder (Fig. 1C, F; Fig. S1D). Whereas MYC overexpression influenced growth kinetics moderately (Fig. S1I) while not affecting basal apoptotic rate or viability (Fig. S1J, K), ectopic MYC expression sensitized Oci-Ly1 to pharmacological SUMO inhibition (Fig. 1F; Fig S1J-L). Moreover, depletion of SUMO signaling by pharmacological or genetic targeting resulted in impaired MYC pathway activity (Fig. S2, Suppl. Table 1).

In summary, we here identify pharmacological SUMO inhibition as a vulnerability and rational treatment strategy for MYC-driven BCL.

### **SUMO inhibition is an effective therapy for MYC-driven B-cell lymphoma *in vivo***

Principal component analysis of mRNA expression of the SUMO core machinery in wild-type (wt) B-cells and MYC-driven BCL from *Eμ-myc* mice confirmed enhanced SUMO pathway expression in MYC-driven BCL (GSE7897) (Fig. S3A). To test whether inhibition of SUMOylation would offer therapeutic efficacy towards MYC-induced BCL, we treated cell lines derived from three independent primary *Eμ-myc* lymphomas with SUMO<sub>i</sub> and detected striking sensitivity to pharmacological inhibition of SUMOylation (Fig. S3B, C). To test therapeutic efficacy *in vivo*, we transplanted primary *Eμ-myc* lymphoma cells into syngeneic wt recipient mice. Seven days after lymphoma cell injection, lymphoma bearing mice received treatment with SUMO<sub>i</sub> or carrier solution (Fig. 2A). CD45.1 and CD45.2 epitope diversity allowed to discriminate between wt recipient B-cells and the syngeneic lymphoma compartment. Strikingly, a single SUMO<sub>i</sub> therapy resulted in a highly efficient reduction and almost complete eradication of *Eμ-myc*-transgenic CD45.2 lymphoma cells in the bone marrow (BM) and spleen (Fig. 2B, C; Fig. S4A). Moreover, a single dose of SUMO<sub>i</sub> treatment

significantly reduced spleen weight without causing obvious signs of severe short-term toxicity (Fig. S4B-D). Thus, we here establish activated MYC signaling as an actionable vulnerability and inhibition of SUMOylation as a rational treatment strategy in a pre-clinical murine model of MYC-driven BCL.

Remarkably, SUMO<sub>i</sub> therapy not only affected the tumor compartment (CD45.2<sup>+</sup>), but phenotype analysis hinted towards major changes in the composition of the recipient primary and secondary lymphoid organs. Analysis of the CD45.1 wt compartment in lymphoma-grafted mice revealed a significant increase in the abundance of CD3<sup>+</sup> T-cells in both BM and spleen after SUMO<sub>i</sub> treatment that was accompanied by a distinct reduction of the recipient B220<sup>+</sup> B-cell compartment, particularly in the spleen (Fig. 2D; Fig. S4E, F), revealing that B-cells were more sensitive to SUMO inhibition than T-cells (Fig. S4G). Besides, the effect on B-cells was less pronounced in recipient B-cells than in MYC-driven lymphoma B-cells (Fig. S4H). The abundance of granulocytes and monocytes mostly remained unaffected by SUMO<sub>i</sub> treatment (Fig. 2D; Fig. S4E, F).

Thus, SUMO inhibition leads to killing of MYC-driven B-cell lymphoma *in vivo*. This fast and most likely direct effect was accompanied by alterations of cellular components of the immune system.

### **SUMO inhibition remodels immune cell abundance *in vivo***

Impaired immune surveillance is involved in lymphoma pathogenesis<sup>27</sup> and induction of immune activity contributes to cancer control<sup>28, 29</sup>. To test if immune effects by SUMO<sub>i</sub> treatment are a general feature independent of presence of lymphoma, we treated C57Bl/6J mice with either SUMO<sub>i</sub> or carrier control on two consecutive days and analyzed splenocytes and BM cells by multicolor flow cytometry (Fig. 3A; Fig. S5A, D). In line with our previous findings in lymphoma bearing mice, SUMO<sub>i</sub> treatment led to a relative increase of the CD3<sup>+</sup>CD4<sup>+</sup> T-cell compartment (Fig. 3B; Fig. S5B, C, E, F). The increase of CD3<sup>+</sup>CD4<sup>+</sup> T-cells, a cellular subset holding an important role in antitumor immunity<sup>30 31</sup>, was most prominent in the spleen. These effects were accompanied by a reduction of the B220<sup>+</sup> B-cell

compartment (Fig. 3B; Fig. S5B, C, E, F, and Fig. S6A, D). Shifts in immune cell abundance were detected in both BM and spleen, despite of a decline in overall BM and spleen cell numbers upon SUMO<sub>i</sub> challenge (Fig. S5A, D).

We next substantiated the *in vivo* effects of pharmacological SUMO<sub>i</sub> on immune cell distribution in more detail. SUMO inhibition resulted in a decline of most B-cell subsets within both primary lymphoid BM tissue and the secondary lymphoid organ spleen (Fig. 3C), which is in line with recent reports<sup>19</sup>. Besides, we detected a significant increase in B220<sup>+</sup> B memory cells after SUMO inhibition in BM and spleen (Fig. 3D; Fig. S6D, S7A), indicating effects on a cellular subset important for a coordinated antibody-dependent immune response<sup>32</sup>.

SUMO-directed intervention not only exerted broad effects on the B-cell subsets, but also on the T-cell compartment, as we observed a significant increase in CD4<sup>+</sup> memory and regulatory T-cells within BM and spleen upon SUMO<sub>i</sub> (Fig. 4A, B; Fig. S6B, E, S7B). Beyond, the abundance of BM CD8<sup>+</sup> effector memory cells was significantly increased (Fig. 4C; Fig. S6C, S7C). Both CD4<sup>+</sup> and CD8<sup>+</sup> T memory cells are antigen-specific long-term persisting cells that arise from naïve T-cells upon encounter to a cognate antigen and are designated to execute a protective immune response upon antigen re-encounter<sup>33, 34</sup>. Of note, SUMO inhibition was accompanied by a substantially higher abundance of activated CD8<sup>+</sup> T-cells (Fig. 4C, D; Fig. S6C, F, S7D), a population referred to as cytotoxic T-cells with well-described features in host defense and tumor cytolysis<sup>35</sup>. This finding is in line with current reports linking SUMO inhibition to enhanced T-cell activation<sup>19, 20, 36</sup>.

In summary, our analyses revealed a substantial remodeling of immune cell subsets following SUMO-directed intervention, underscoring the important role of the SUMO pathway in the immune system.

### **SUMO inhibition substantially alters the normal B-cell landscape**

Our preceding analyses revealed pharmacologic inhibition of SUMOylation as a vulnerability in MYC-driven lymphoma that was associated with pronounced changes in the immune cell

compartment. To decipher the effects of short term highly specific small molecule SUMO<sub>i</sub> on B-cell subsets in more detail, we next opted for Cellular Indexing of Transcriptomes and Epitopes by Sequencing (CITE-seq) analysis (dataset GSE193359)<sup>20</sup>. CITE-seq combines the measurements of surface protein levels and transcriptome analysis to determine cellular states and their alterations at single-cell level<sup>37</sup>. In this experiment wt mice were challenged with a lower dose of the SUMO inhibitor subasumstat in line with a recent publication reporting enhanced anti-tumor T-cell capacity upon SUMO<sub>i</sub><sup>36</sup>. CITE-seq analysis was conducted on spleens from 3 control and 3 SUMO<sub>i</sub>-treated mice. Prior to analysis cells were marked with oligo-conjugated antibodies allowing discrimination between B- and T-cell subsets (Fig. 5A). Transcriptomics and surface proteomics was conducted on the 10x Genomics platform. In total 18361 cells (9878 cell from control mice and 8483 from SUMO<sub>i</sub> treated mice) were analyzed. Using expression data of B-cell surface markers and B-cell specific marker genes, we annotated 11 different murine B-cell populations (Fig. 5B; Fig. S8). SUMO<sub>i</sub> treatment resulted in decreased abundance of the early and more immature splenic B-cell subset T1 and T3 (Fig. S9A). The abundance of memory and marginal zone B-cells was substantially higher in SUMO<sub>i</sub> treated mice (Fig. 5C, D). Moreover, we detected a striking decline in dark zone and light zone B-cells (Fig. 5C, D). Of note, MYC expression is induced in light-zone B-cells in direct proportion to antigen capture during the dark-zone to light-zone germinal center transition to coordinate residence time in the dark-zone<sup>38</sup>. Accordingly, we observed high expression of the MYC core machinery in light-zone B-cells that was associated with enhanced expression of the SUMO core machinery (Fig. 5E). Remarkably, SUMO inhibition abrogated this effect (Fig. 5F; Fig. S9B). Assessing the question of whether cellular proliferation needs to be considered as a confounder effect when evaluating the changes in abundance between treatment conditions, we performed proliferation score analysis on B- and T-cells within the CITE-seq dataset (Fig. S10A, B, D-F). Differences in proliferation among the different cell populations were overall moderate and not significantly altered after SUMO inhibition among all subsets analyzed (Fig. S10C).

In summary, these data revealed the complexity of a SUMO-directed therapeutic intervention on immune cell abundance and specifically on the B-cell landscape. Furthermore, we could link MYC expression to expression of the SUMO core machinery on a single-cell level, highlighting MYC signaling as an actionable vulnerability targeted by SUMO inhibition.

## DISCUSSION

Here, we unraveled activation of SUMOylation as a striking vulnerability in MYC-driven BCL. Next to direct effects of specific pharmacological SUMO inhibition on MYC-induced lymphoma, our investigations depicted a substantial remodeling of components of the innate and specific immunity *in vivo* by SUMOi.

Defining strategies to tackle MYC-driven tumors is of huge relevance based on the well-established activation of MYC in the vast majority of cancers, however, direct MYC targeting remains challenging<sup>39</sup>. Although MYC targeting via a dominant-negative peptide OMOMYC showed promising preclinical results and is currently tested in a phase1/2 clinical trial (NCT04808362)<sup>40</sup>, no direct MYC inhibitor has reached clinical practice<sup>8</sup>. These unmet challenges favor the idea of targeting deregulated cellular pathways in MYC-overexpressing tumors to translate the concept of “synthetic lethality”<sup>7,8</sup> into clinical cancer therapy. We here identified aberrant activity of the SUMO core pathway in aggressive BCL with activated MYC signaling and identified activated MYC signaling as an actionable molecular vulnerability *in vitro* and in a pre-clinical murine model of MYC-driven lymphoma *in vivo*. Notably, SUMO inhibition alone or administered as combination therapy with rituximab, a standard therapy for BCL patients, showed remarkable efficacy in preclinical DLBCL xenograft models<sup>25, 41</sup>. Besides, SUMO inhibition is currently tested in various clinical trials (NCT03648372, NCT04074330, NCT04381650), emphasizing the relevance of our findings for biomarker-informed clinical applications. Our data is in line with an unbiased synthetic lethality screen in MYC-driven breast cancer that uncovered a role for the SUMO activation complex SAE1/2 in MYC-driven tumorigenesis<sup>21</sup>. Furthermore, a previous loss-of-function study in BCL linked silencing of SAE2 to tumor regression *in vivo*<sup>22</sup>. The MYC-SUMO connection and MYC-

related sensitivity to SUMO<sub>i</sub> was also identified in aggressive pancreatic cancer<sup>23</sup>. We here provide first data indicating that highly specific small molecule SUMO inhibition is an effective therapy for MYC-driven BCL *in vivo* and demonstrate a key role for activated MYC signaling in conferring susceptibility to SUMO inhibition in B-cells, while non-cancer syngeneic B-cells showed remarkably lower killing rates as compared to the MYC-driven lymphoma population. This MYC-dependent effect of SUMO inhibition was confirmed by ectopic expression of MYC in the human DLBCL cells. Moreover, following *in vivo* low dose SUMO<sub>i</sub> challenge, CITE-seq analysis showed diminished abundance of wt light-zone B-cells that are characterized by high MYC expression and concurrent high expression of the SUMO core machinery. Beyond depicting MYC signaling as a vulnerability, we would like to emphasize that uncovering additional biomarkers predicting SUMO<sub>i</sub> sensitivity in cancer therapy is an area worthy of further investigations.

Apart from driving cancer progression through tumor-cell intrinsic acquisition of cancer hallmarks, MYC restrains the anticancer immune response and dysregulates the tumor microenvironment<sup>27, 42</sup>. We show substantial alteration of the B-cell landscape upon SUMO inhibition in a wild-type mouse model and report higher abundance of memory B-cells after pharmacological SUMO inhibition, accompanied by a decline in immature subsets, which is in line with recent publications<sup>19</sup>. B memory cells are accounted with a key role in sustaining a long-term immune response<sup>32, 43</sup>. SUMO inhibition not only altered B-cell abundance, but also strikingly increased the abundance of CD8<sup>+</sup> cytotoxic T-cells as well as CD4<sup>+</sup> and CD8<sup>+</sup> memory T-cells and particularly T-regulatory cells. CD8<sup>+</sup> effector T-cells exert direct antitumor cytotoxicity and CD4<sup>+</sup> T-cells enhance cytolytic efficacy of CTLs by antigen cross-presentation and mediate plasma cell differentiation<sup>30, 31, 35</sup>. T-regulatory cells are accounted with a double-edged role in anti-tumor immunity<sup>44</sup>. They suppress anti-cancer immunity, but also drive and control the T-cell immune responses against tumor neoantigens<sup>45</sup>. So far, only enhanced CD8<sup>+</sup> T-cell activation and augmented anti-tumor sensitivity by SUMO<sub>i</sub>-mediated reactivation of type I interferon signaling have been reported before<sup>19, 20, 36</sup>. We here identified

a novel function of SUMO inhibition in remodeling the immune cell landscape by enhancing abundance of cellular subsets involved in the innate and specific immune response.

In summary, we here depict activated MYC signaling as an actionable molecular vulnerability for SUMO inhibition *in vitro* and in a pre-clinical murine model of MYC-driven BCL *in vivo*.

Next to direct effects on MYC-driven lymphoma, SUMO inhibition substantially remodels the immune cell landscape *in vivo* independent of a tumor microenvironment. Our findings thus identify SUMO inhibition as a powerful therapy in a subset of MYC-driven BCLs and suggest SUMO-targeted therapies as a potential therapeutic strategy for cancer immunotherapy.

## REFERENCES

1. Dang CV. MYC on the path to cancer. *Cell*. 2012;149(1):22-35.
2. Schick M, Habringer S, Nilsson JA, Keller U. Pathogenesis and therapeutic targeting of aberrant MYC expression in haematological cancers. *Br J Haematol*. 2017;179(5):724-738.
3. Chen H, Liu H, Qing G. Targeting oncogenic Myc as a strategy for cancer treatment. *Signal Transduct Target Ther*. 2018;3:5.
4. Singh K, Lin J, Zhong Y, et al. c-MYC regulates mRNA translation efficiency and start-site selection in lymphoma. *J Exp Med*. 2019;216(7):1509-1524.
5. Ruggero D. The role of Myc-induced protein synthesis in cancer. *Cancer Res*. 2009;69(23):8839-8843.
6. Stine ZE, Walton ZE, Altman BJ, Hsieh AL, Dang CV. MYC, Metabolism, and Cancer. *Cancer Discov*. 2015;5(10):1024-1039.
7. Kaelin WG, Jr. The concept of synthetic lethality in the context of anticancer therapy. *Nat Rev Cancer*. 2005;5(9):689-698.
8. Dhanasekaran R, Deutzmann A, Mahauad-Fernandez WD, Hansen AS, Gouw AM, Felsher DW. The MYC oncogene - the grand orchestrator of cancer growth and immune evasion. *Nat Rev Clin Oncol*. 2022;19(1):23-36.
9. Seeler JS, Dejean A. SUMO and the robustness of cancer. *Nat Rev Cancer*. 2017;17(3):184-197.
10. Hendriks IA, Vertegaal AC. A comprehensive compilation of SUMO proteomics. *Nat Rev Mol Cell Biol*. 2016;17(9):581-595.
11. Flotho A, Melchior F. Sumoylation: a regulatory protein modification in health and disease. *Annu Rev Biochem*. 2013;82:357-385.
12. Cappadocia L, Lima CD. Ubiquitin-like Protein Conjugation: Structures, Chemistry, and Mechanism. *Chem Rev*. 2018;118(3):889-918.
13. Kunz K, Piller T, Muller S. SUMO-specific proteases and isopeptidases of the SENP family at a glance. *J Cell Sci*. 2018;131(6);jcs211904.
14. Bawa-Khalfe T, Yeh ET. SUMO Losing Balance: SUMO Proteases Disrupt SUMO Homeostasis to Facilitate Cancer Development and Progression. *Genes Cancer*. 2010;1(7):748-752.
15. Schick M, Zhang L, Maurer S, et al. Genetic alterations of the SUMO isopeptidase SENP6 drive lymphomagenesis and genetic instability in diffuse large B-cell lymphoma. *Nat Commun*. 2022;13(1):281.
16. Driscoll JJ, Pelluru D, Lefkimiatis K, et al. The sumoylation pathway is dysregulated in multiple myeloma and is associated with adverse patient outcome. *Blood*. 2010;115(14):2827-2834.
17. Sun WC, Hsu PI, Yu HC, et al. The compliance of doctors with viral hepatitis B screening and antiviral prophylaxis in cancer patients receiving cytotoxic chemotherapy using a hospital-based screening reminder system. *PLoS One*. 2015;10(2):e0116978.
18. Decque A, Joffre O, Magalhaes JG, et al. Sumoylation coordinates the repression of inflammatory and anti-viral gene-expression programs during innate sensing. *Nat Immunol*. 2016;17(2):140-149.
19. Kumar S, Schoonderwoerd MJA, Kroonen JS, et al. Targeting pancreatic cancer by TAK-981: a SUMOylation inhibitor that activates the immune system and blocks cancer cell cycle progression in a preclinical model. *Gut*. 2022 Jan 24. [Epub ahead of print]
20. Demel UM, Boger M, Yousefian S, et al. Activated SUMOylation restricts MHC class I antigen presentation to confer immune evasion in cancer. *J Clin Invest*. 2022;132(9):e152383.
21. Kessler JD, Kahle KT, Sun T, et al. A SUMOylation-dependent transcriptional subprogram is required for Myc-driven tumorigenesis. *Science*. 2012;335(6066):348-353.
22. Hoellein A, Fallahi M, Schoeffmann S, et al. Myc-induced SUMOylation is a therapeutic vulnerability for B-cell lymphoma. *Blood*. 2014;124(13):2081-2090.
23. Biederstadt A, Hassan Z, Schneeweis C, et al. SUMO pathway inhibition targets an aggressive pancreatic cancer subtype. *Gut*. 2020;69(8):1472-1482.

24. He X, Riceberg J, Soucy T, et al. Probing the roles of SUMOylation in cancer cell biology by using a selective SAE inhibitor. *Nat Chem Biol.* 2017;13(11):1164-1171.
25. Langston SP, Grossman S, England D, et al. Discovery of TAK-981, a First-in-Class Inhibitor of SUMO-Activating Enzyme for the Treatment of Cancer. *J Med Chem.* 2021;64(5):2501-2520.
26. Doffo J, Bamopoulos SA, Kose H, et al. NOXA expression drives synthetic lethality to RUNX1 inhibition in pancreatic cancer. *Proc Natl Acad Sci U S A.* 2022;119(9):e2105691119.
27. Casey SC, Baylot V, Felsher DW. The MYC oncogene is a global regulator of the immune response. *Blood.* 2018;131(18):2007-2015.
28. Kubli SP, Berger T, Araujo DV, Siu LL, Mak TW. Beyond immune checkpoint blockade: emerging immunological strategies. *Nat Rev Drug Discov.* 2021;20(12):899-919.
29. Restifo NP, Dudley ME, Rosenberg SA. Adoptive immunotherapy for cancer: harnessing the T cell response. *Nat Rev Immunol.* 2012;12(4):269-281.
30. Borst J, Ahrends T, Babala N, Melief CJM, Kastenmuller W. CD4(+) T cell help in cancer immunology and immunotherapy. *Nat Rev Immunol.* 2018;18(10):635-647.
31. Tay RE, Richardson EK, Toh HC. Revisiting the role of CD4(+) T cells in cancer immunotherapy-new insights into old paradigms. *Cancer Gene Ther.* 2021;28(1-2):5-17.
32. Sautes-Fridman C, Petitprez F, Calderaro J, Fridman WH. Tertiary lymphoid structures in the era of cancer immunotherapy. *Nat Rev Cancer.* 2019;19(6):307-325.
33. Martin MD, Badovinac VP. Defining Memory CD8 T Cell. *Front Immunol.* 2018;9:2692.
34. Stockinger B, Bourgeois C, Kassiotis G. CD4+ memory T cells: functional differentiation and homeostasis. *Immunol Rev.* 2006;211:39-48.
35. St Paul M, Ohashi PS. The Roles of CD8(+) T Cell Subsets in Antitumor Immunity. *Trends Cell Biol.* 2020;30(9):695-704.
36. Lightcap ES, Yu P, Grossman S, et al. A small-molecule SUMOylation inhibitor activates antitumor immune responses and potentiates immune therapies in preclinical models. *Sci Transl Med.* 2021;13(611):eaba7791.
37. Stoeckius M, Hafemeister C, Stephenson W, et al. Simultaneous epitope and transcriptome measurement in single cells. *Nat Methods.* 2017;14(9):865-868.
38. Finkin S, Hartweger H, Oliveira TY, Kara EE, Nussenzweig MC. Protein Amounts of the MYC Transcription Factor Determine Germinal Center B Cell Division Capacity. *Immunity.* 2019;51(2):324-336.
39. Schneider G, Wirth M, Keller U, Saur D. Rationale for MYC imaging and targeting in pancreatic cancer. *EJNMMI Res.* 2021;11(1):104.
40. Llombart V, Mansour MR. Therapeutic targeting of "undruggable" MYC. *EBioMedicine.* 2022;75:103756.
41. Nakamura A, Grossman S, Song K, et al. The SUMOylation inhibitor subasumstat potentiates rituximab activity by IFN1-dependent macrophage and NK cell stimulation. *Blood.* 2022;139(18):2770-2781.
42. Seton-Rogers S. Oncogenes: Driving immune evasion. *Nat Rev Cancer.* 2018;18(2):67.
43. Sharonov GV, Serebrovskaya EO, Yuzhakova DV, Britanova OV, Chudakov DM. B cells, plasma cells and antibody repertoires in the tumour microenvironment. *Nat Rev Immunol.* 2020;20(5):294-307.
44. Togashi Y, Shitara K, Nishikawa H. Regulatory T cells in cancer immunosuppression - implications for anticancer therapy. *Nat Rev Clin Oncol.* 2019;16(6):356-371.
45. Pace L, Tempez A, Arnold-Schrauf C, et al. Regulatory T cells increase the avidity of primary CD8+ T cell responses and promote memory. *Science.* 2012;338(6106):532-536.

## FIGURE LEGENDS

**Figure 1. Active MYC signaling confers susceptibility to small molecule SUMO inhibition in DLBCL cell lines.**

- A) Hierarchical clustering (Euclidean/Ward) of indicated SUMO core components of normalized human DLBCL transcriptome profiles (GSE98588) revealed SUMO<sup>high</sup> and SUMO<sup>low</sup> subgroups as indicated.
- B) Gene set enrichment analysis of SUMO<sup>high</sup> and SUMO<sup>low</sup> subgroups using Hallmark gene sets from the molecular signature database (MSigDb). Indicated MYC target gene signatures have been identified using GeneTrail v3 (Kolgomorov-Smirnov-Test). Adjusted p-values (q) are indicated.
- C) Flow cytometry analysis of relative viability of indicated DLBCL cell lines treated with increasing SUMO<sub>i</sub> concentrations (Tak-981, 0, 3.9, 7.8, 15.6, 31.2, 62.5, 125, 250, 500, 1000, 2000nM) for 72h (n=3).
- D) Gene set enrichment analysis of SUMO<sub>i</sub>-responder (Oci-Ly19, SU-DHL-5, SU-DHL-8) vs. SUMO<sub>i</sub>-non-responder (U-2932, SU-DHL-4, DB, NU-DHL-1) on expression profiles accessed via GSE53798. Enrichment plot on SUMOylation signatures, obtained from the Reactome knowledgebase. Adjusted p-values (q) are indicated. Volcano plot displays significant gene signatures of the Hallmark gene set (MSigDb) with both MYC Hallmark signatures (V1, V2) highlighted.
- E) Enrichment plot on MYC Hallmark signatures, based on the analysis described in (D). Adjusted p-values (q) are indicated.
- F) Relative viability of Oci-Ly1 cells transduced with a MYC expression plasmid or a control plasmid, treated with increasing SUMO<sub>i</sub> concentrations (Tak-981, 0, 3.9, 7.8, 15.6, 31.2, 62.5, 125, 250, 500, 1000, 2000nM) for 72h (n=3). P-value refers to 2000nM SUMO<sub>i</sub> and is determined by unpaired t-test. Immunoblot analysis of Oci-Ly1 control and MYC cell lines.

**Figure 2. SUMO inhibition is an effective therapy for Myc-driven B-cell lymphoma *in vivo*.**

- A) Schematic illustration showing transplantation of *Eμ-myc* lymphoma cells (CD45.2) into wildtype (CD45.1) recipient mice. Mice were treated with carrier or SUMO<sub>i</sub> (ML-093, 50mg/kg) at day 7 post transplantation. Analysis of bone marrow, spleen and blood was performed at day 9, n=6 per condition.
- B) Pie charts representing the frequencies of wt and *Eμ-myc* lymphoma cells in the bone marrow (BM) and spleen after carrier vs. SUMO<sub>i</sub> treatment.

- C) Total number of *Eμ-myc* lymphoma cells in the BM and spleen following SUMO $\text{i}$  treatment compared to carrier. N=6, *P-values* was determined by unpaired t-test.
- D) Pie charts representing the frequencies of B-cells (B220 $^+$ ), T-cells (CD3 $^+$ ), granulocytes (Gr.1 $^+$ CD11b $^+$ ) and monocytes (Gr.1 $^+$ CD11b $^+$ ) in the BM and spleen after carrier vs. SUMO $\text{i}$  treatment.

**Figure 3. SUMO inhibition induces major changes in the B-cell compartment, favoring a memory B-cell phenotype.**

- A) Schematic illustration showing treatment of wt mice with carrier or SUMO $\text{i}$  (ML-093, 50mg/kg) at day 1 and 2. Analysis of BM and spleen was performed at day 3, n=6 per condition.
- B) Pie charts representing the frequencies of indicated cell populations (B220 $^+$  B-cells, CD3 $^+$ CD4 $^+$  T-cells, CD3 $^+$ CD8 $^+$  T-cells) in the BM and spleen after carrier vs. SUMO $\text{i}$  treatment.
- C) Pie charts representing the frequencies of indicated cell populations in the B220 $^+$  BM compartment (B220 $^+$ IgM $^-$  Pre-Pro B-cells, B220 $^+$ IgM $^+$ IgD $^-$  Immature B-cells, B220 $^+$ CD19 $^+$ MHC-II $^+$  Activated B-cells, B220 $^+$ CD80 $^+$ CD86 $^+$  Memory B-cells) and B220 $^+$  spleen compartment (B220 $^+$ CD93 $^+$  Immature B-cells, B220 $^+$ CD21 $^{\text{high}}$ CD23 $^{\text{low}}$  Marginal zone B-cells, B220 $^+$ CD21 $^{\text{low}}$ CD23 $^{\text{high}}$  Follicular B-cells, B220 $^+$ CD80 $^+$ CD86 $^+$  Memory B-cells, B220 $^+$ CD19 $^+$ MHC-II $^+$  Activated B-cells) after carrier vs. SUMO $\text{i}$  treatment.
- D) Percentage of Memory B-cells (B220 $^+$ CD21 $^{\text{high}}$ CD23 $^{\text{low}}$ ) of B220 $^+$  BM and spleen cells. N=6, *p-values* were determined by unpaired t-test.

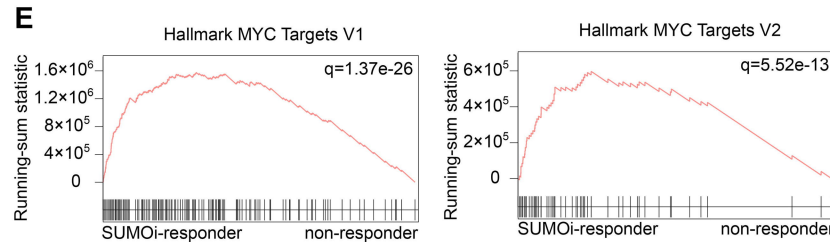
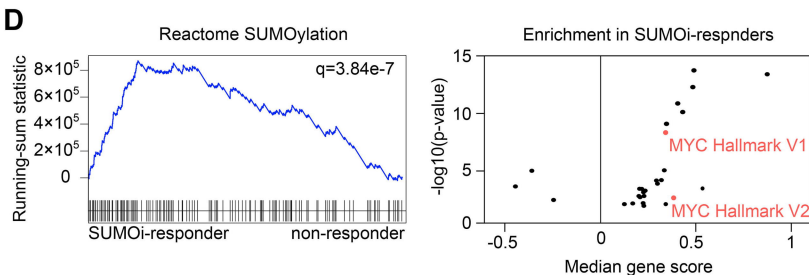
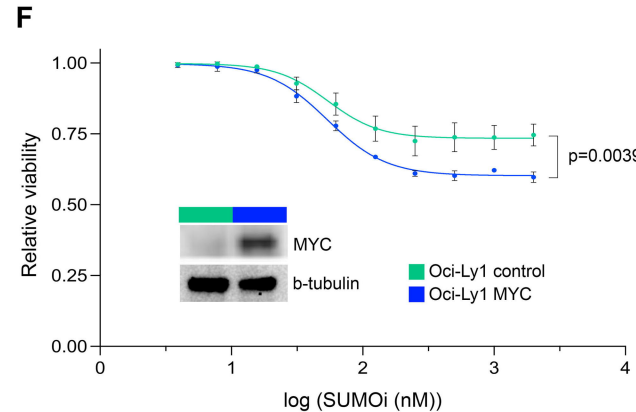
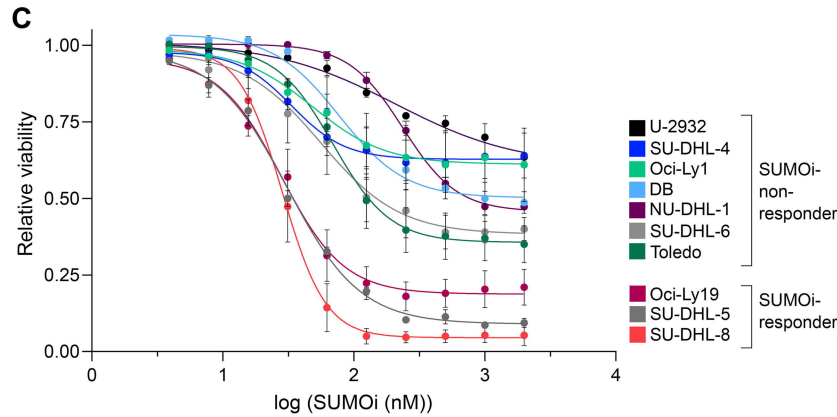
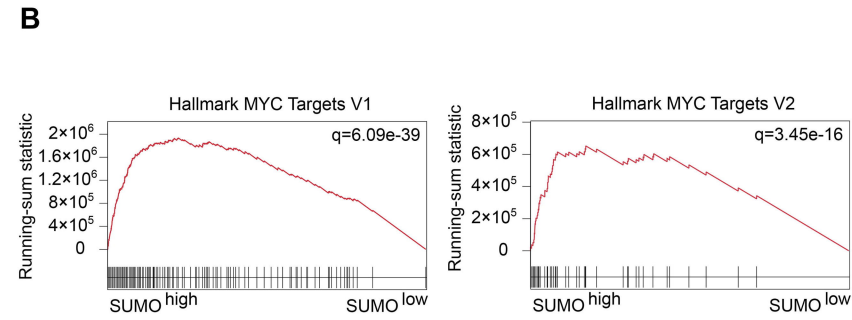
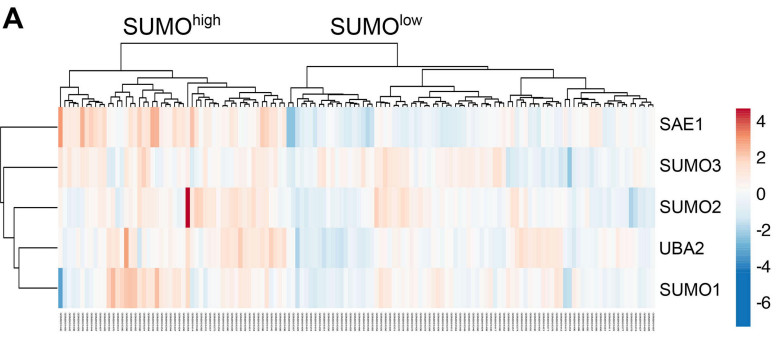
**Figure 4. SUMO inhibition remodels the T-cell compartment towards a memory and activated T-cell phenotype.**

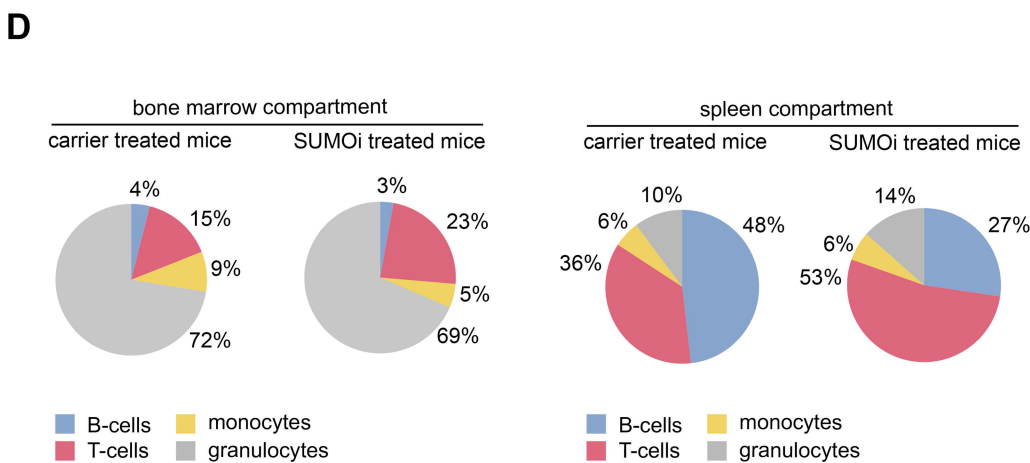
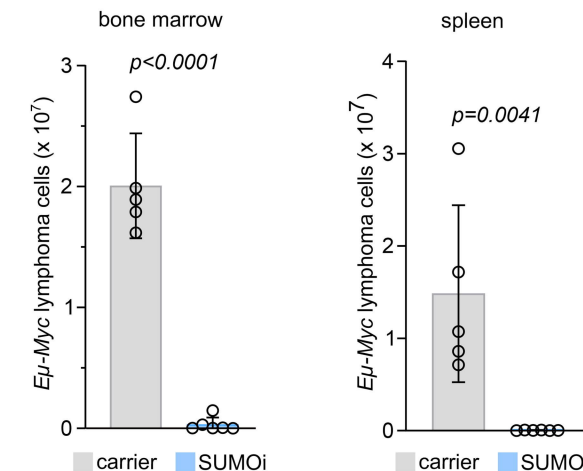
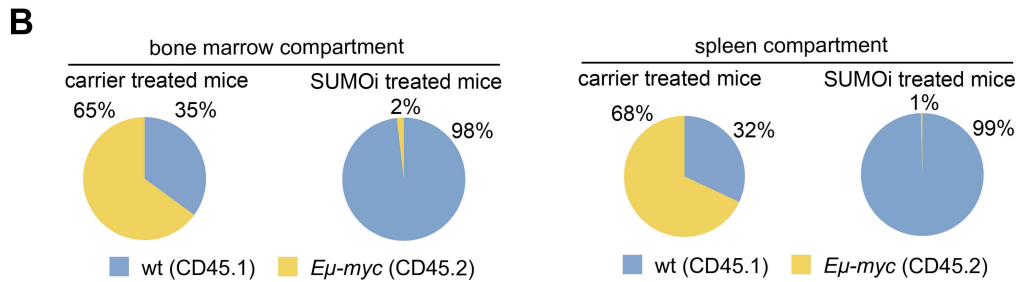
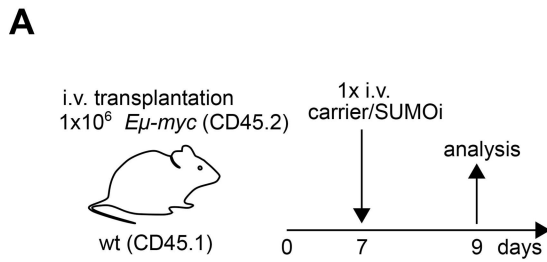
- A) Experimental setup as outlined in Fig. 3A. Pie charts representing the frequencies of the indicated cell populations in the CD3 $^+$ CD4 $^+$  BM and spleen compartment (CD3 $^+$ CD4 $^+$ CD44 $^{\text{low}}$ CD62L $^+$  Naïve T-cells, CD3 $^+$ CD4 $^+$ CD44 $^{\text{high}}$ CD62L $^-$  Memory T-Cells, CD3 $^+$ CD4 $^+$ CD44 $^{\text{low}}$ CD62L $^-$  Effector T-cells, CD3 $^+$ CD4 $^+$ CD25 $^+$ CD69 $^+$ FoxP3 $^+$  Regulatory T-cells).
- B) Percentage of Memory T-cells (CD3 $^+$ CD4 $^+$ CD44 $^{\text{high}}$ CD62L $^-$ ) of the CD3 $^+$ CD4 $^+$  BM and spleen cells. N=6, *p-values* were determined by unpaired t-test.
- C) Pie charts representing the frequencies of the indicated cell populations in the CD3 $^+$ CD8 $^+$  BM and spleen compartment (CD3 $^+$ CD8 $^+$ CD44 $^{\text{low}}$ CD62L $^+$  Naïve T-cells, CD3 $^+$ CD8 $^+$  CD44 $^{\text{high}}$ CD62L $^-$  Effector Memory T-Cells, CD3 $^+$ CD8 $^+$ CD44 $^{\text{high}}$ CD62L $^+$

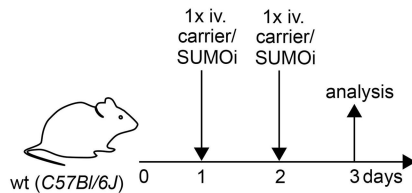
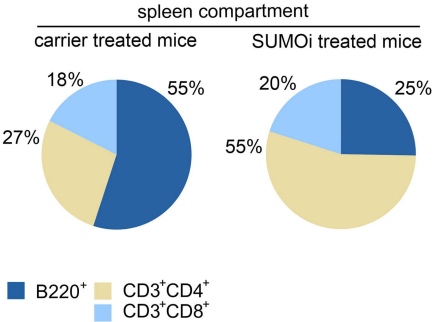
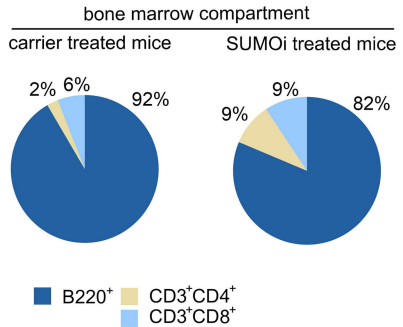
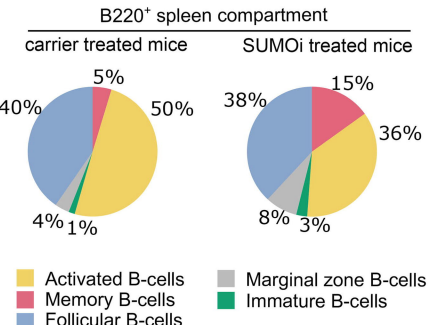
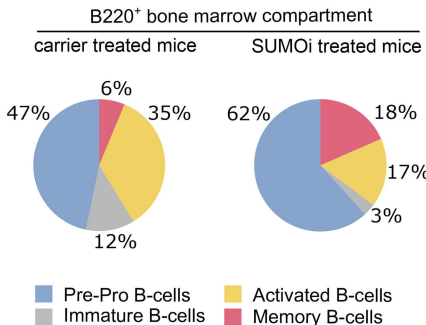
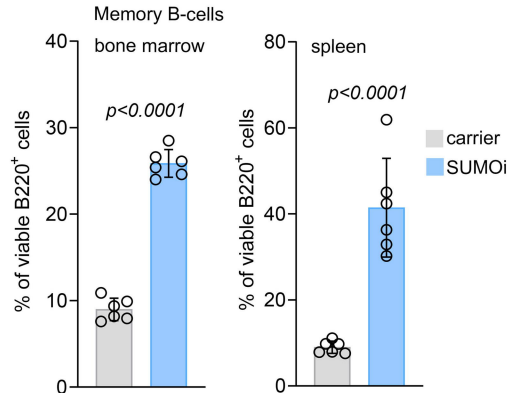
- Central Memory T-cells, CD3<sup>+</sup>CD8<sup>+</sup>CD25<sup>+</sup>CD69<sup>+</sup> Activated T-cells) after carrier vs. SUMO<sub>i</sub> treatment.
- D) Percentage of Activated T-cells (CD3<sup>+</sup>CD8<sup>+</sup>CD25<sup>+</sup>CD69<sup>+</sup>) of the CD3<sup>+</sup>CD8<sup>+</sup> BM and spleen cells. N=6, *p*-values were determined by unpaired t-test.

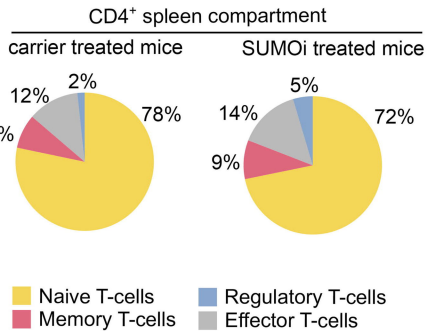
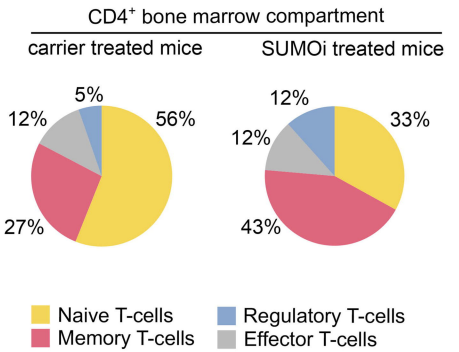
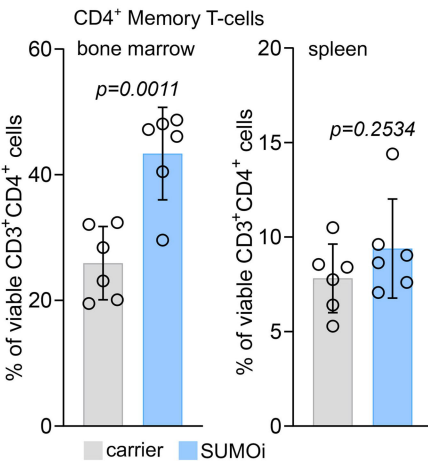
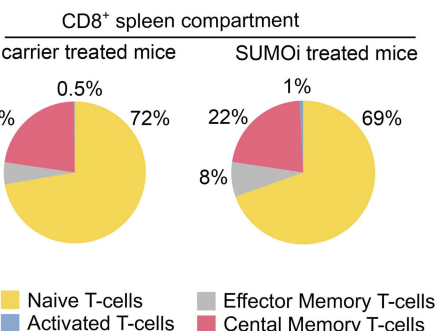
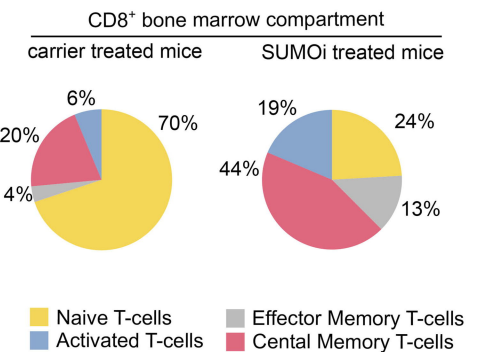
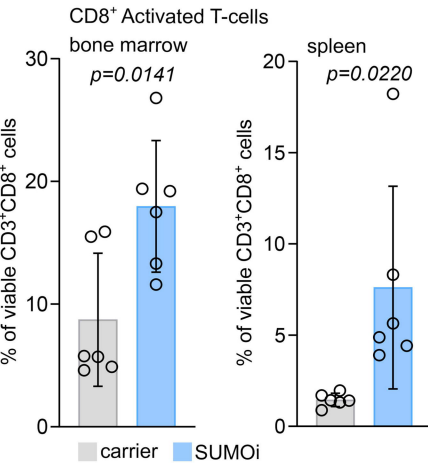
**Figure 5. SUMO inhibition substantially alters the normal B cell landscape.**

- A) UMAP visualization of spleen scRNA-seq data from control and SUMO<sub>i</sub>-treated mice (subasumstat 7.5mg/kg on day 1 and 4, spleen cell analysis day 5; dataset GSE193359).
- B) B-cell populations identified in (A) were subsetted and reclustered. The UMAP visualization represents B-cells from both conditions.
- C) Differentially abundant B-cell populations in control and SUMO<sub>i</sub> treated mice identified with DA-seq. Cells are colored by DA-seq measure. Yellow = more abundant after SUMO<sub>i</sub> challenge. Dark blue = more abundant after control treatment.
- D) Differential abundance testing on mouse-wise pseudobulks (indicated by white dots, n=3). Bar plots represent the subpopulation frequencies stratified by condition. The median is indicated by the center line of the box plot. The box extends from the 25<sup>th</sup> to 75<sup>th</sup> percentiles, whisker length reaches from minimum to maximum. Significance is determined by a Negative Binomial Generalized Linear Model.
- E) SUMO and MYC score correlation analysis in control mice. Scaled mean expression values are plotted against each other for each cell population identified in Fig. 5B. R indicates the Pearson correlation coefficient. The regression line is shown in black. The grey area indicates the 95% confidence interval.
- F) SUMO and MYC score correlation analysis in control and SUMO<sub>i</sub> treated mice. For each population the Pearson correlation coefficient (R) is plotted. Black bars indicate the range of the 95% confidence interval. The dashed black line at R = 0 is a reference line and plotted as a visualization aid.





**A****B****C****D**

**A****B****C****D**

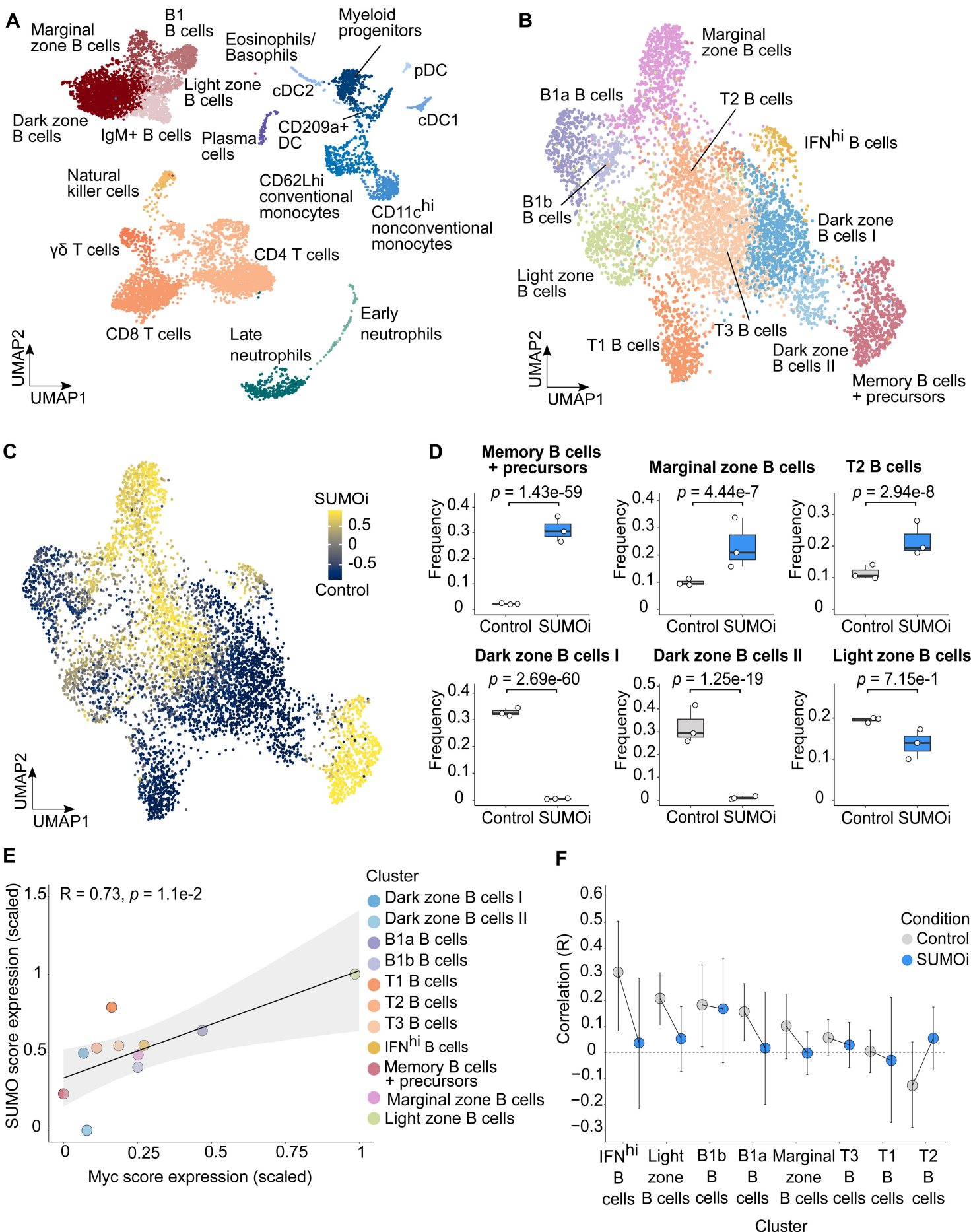


Figure 5. SUMO inhibition substantially alters the normal B cell landscape.

# **Small molecule SUMO inhibition for biomarker-informed B-cell lymphoma therapy**

Demel et al.

## SUPPLEMENTARY METHODS

### Transcriptome profiling and processing of gene expression data

Transcriptome data from human DLBCL patient samples was downloaded from the gene expression omnibus (GEO) database as CEL files of datasets GSE98588 and GSE34171<sup>1 2</sup>. Gene expression data of DLBCL cell lines, which were experimentally divided into SUMOi-responder cells (Oci-LY19, SU-DHL-5, SU-DHL-8) and SUMOi-non-responder cells (U-2932, SU-DHL-4, DB, NU-DHL-1) was accessed via the GEO accession number GSE53798<sup>3</sup>. Transcriptome data from murine *Eμ-Myc* induced lymphomas and healthy B-cells was accessed via GSE7897<sup>4</sup>. The CEL files of the Affymetrix Human Genome U133 arrays or Affymetrix Mouse Genome 430 2.0 arrays were processed using Expression Console software (Affymetrix). Data was normalized using the robust multi-array algorithm (RMA), log2 transformed and probes were collapsed. Z-scores were generated from the expression matrices and identifiers of the SUMO core machinery were used for further cluster analyses. *SUMO1*, *SUMO2*, *SUMO3*, *UBA2*, and *SAE1* identifiers were used to generate the SUMO<sup>high</sup> and SUMO<sup>low</sup> clusters within the GSE98588 dataset. Accordingly, SUMO<sup>high</sup> and SUMO<sup>low</sup> clusters were generated within the GSE34171 dataset, including canonical MYC targets (*ODC1*, *NCL*, *CAD*, *MYC*). Clinical data was used for survival analysis visualized by Kaplan-Meier plots. Statistical comparison of the two survival curves was performed using a log-rank test. Hierarchical clustering was performed according to the Euclidean distance and Ward method for both columns and rows using ClustVis software<sup>5</sup>. The resulting unbiased dichotomization into the two main groups SUMO<sup>low</sup> and SUMO<sup>high</sup> was used to subject the respective samples to gene set enrichment analysis of log2 transformed data. For the GSEA of the DLBCL cell lines as well as the transcriptome data of the *Eμ-myc* lymphomas, log2 transformed expression values were used. The respective groups from the used datasets were analyzed using GeneTrail3.0 software (Kolgomorov-Smirnov test)<sup>6</sup> and the Hallmark and Reactome gene signatures from the Molecular Signature Database (MSigDb)<sup>7</sup>. The generated results were graphically visualized in a volcano plot or in a GSEA plot, generated with GraphPadPrism software v9. Within the *Eμ-myc* dataset, the SUMO core machinery identifiers

were used for principal component analysis (PCA). The PCA plot was generated using ClustVis software<sup>5</sup>.

### **Single Cell RNA-seq analysis**

**Quality assessment of scRNA-seq data.** For this part of the study, we used the publicly available CITE-seq dataset of SUMO*i* treated C57Bl6 mice (GSE193359). Count matrices were imported into R (version 4.1.0) and processed with the Seurat package (4.0.5). Cells with  $\geq 200$  detected genes and containing  $< 10\%$  mitochondrial reads were retained for further analysis. Outlier cells were removed by applying upper filtering thresholds for the number of genes and UMIs which were set to  $\geq 6,000$  and  $\geq 40,000$ , respectively. Moreover, genes captured in  $< 3$  cells were removed from the count matrix. Samples were demultiplexed based on the HTO expression and only singlets were included in subsequent analyses. HTO demultiplexing was performed using Seurat's HTODemux function with default parameters. A preliminary clustering of non-integrated data was conducted and signature genes for each cluster were determined using Seurat's FindMarker function. Cell populations that co-expressed marker genes for distinct cell types, were defined as doublet clusters and removed prior to data integration. Additionally, to remove contamination of ambient RNA in single cells, decontX<sup>8</sup> was independently applied for each batch with default parameters. The decontaminated count matrices were used for all downstream analyses.

**Data integration, clustering and cell type annotation.** Following quality assessment and selection of high-quality cells, samples were integrated to remove batch effects. For this, Seurat's standard integration workflow was applied. Initially, decontaminated RNA counts were log-normalized to account for library size differences and the top 2,000 variable genes were determined. Subsequently, integration features were determined, and integration anchors selected using CCA (canonical correlation analysis) and mutual nearest neighbors (MNN)<sup>9</sup>. After integration, the object was scaled, and a principal component analysis (PCA) performed. The top 30 principal components were selected for shared nearest neighbor (SNN) graph construction, clustering (using the Louvain algorithm) and UMAP visualization. To find

signature genes for each cluster, Seurat's FindMarker function was applied. Spleen cell populations were manually annotated based on knowledge-derived gene lists and marker genes. B cells from both conditions were subsetted and reclustered using the top 20 PCs as described above.

**Differential abundance analysis.** DA-seq<sup>10</sup> was applied to identify differentially abundant B cell populations between the conditions. The analysis was performed based on the instructions in the DA-seq tutorial (on <https://klugerlab.github.io/DASEQ/articles/tutorial.html>) with values for k ranging from 20 to 500. As DA-seq does not provide any statistical output, a differential abundance testing of B cell clusters was conducted using mouse-wise pseudobulks. In brief, cell numbers for each sample (mouse) and cluster were determined. In the next step, the cell type frequencies were calculated for each population and sample by dividing the respective cell number by the total number of cells within that cluster. To determine statistical significance, design and contrast matrices were generated using the model.matrix (stats package version 4.1.0) and makeContrasts function (limma package version 3.48.1). The glmFit function (edgeR package version 3.34.0) was used to fit a Negative Binomial Generalized Linear Model and likelihood ratio tests were performed using glmLRT (edgeR package).

**Sumo-Myc correlation analysis.** Given the comparatively high degree of sparsity in single-cell RNA-seq data, the following analysis used module scores for Sumo and Myc expression, respectively. To generate these gene scores, Seurat's AddModuleScore function was utilized. The *Sumo* score consisted of the six SUMO core machinery genes: *Sumo1*, *Sumo2*, *Sumo3*, *Sae1*, *Uba2*, *Ube2i*. For the *Myc* score, the “hallmark *Myc* targets V2” gene list was used (<https://www.gsea-msigdb.org>). The AddModuleScore function was run independently for each condition and the mean score expression per cluster and condition was calculated. Mean expression values were then scaled from 0-1 (condition-wise) by applying a min-max scaling (highest expression value = 1, lowest expression value 0). The scaled mean expression values of both scores were plotted against each other for each cell population and the Pearson correlation coefficient (R) was calculated using the stat\_cor function (ggpubr package 0.4.0). In addition, we studied how SUMO*i* treatment would affect the correlation of Sumo and Myc

module scores. To do so, the correlation ( $R$ ) between Sumo and Myc scores were calculated for each population condition-wise. Cell cluster with <50 cells in one of the conditions were excluded from this analysis.

**Analysis of cell proliferation.** The expression of a cell proliferation score was used to assess whether certain cell populations are more proliferative active. The proliferation score was generated with Seurat's AddModuleScore function using genes from the GSEA gene set "cell\_proliferation\_GO\_0008283".

## SUPPLEMENTARY REFERENCES

1. Chapuy B, Stewart C, Dunford AJ, et al. Molecular subtypes of diffuse large B cell lymphoma are associated with distinct pathogenic mechanisms and outcomes. *Nat Med.* 2018;24(5):679-690.
2. Monti S, Chapuy B, Takeyama K, et al. Integrative analysis reveals an outcome-associated and targetable pattern of p53 and cell cycle deregulation in diffuse large B cell lymphoma. *Cancer Cell.* 2012;22(3):359-372.
3. Falgreen S, Dybkaer K, Young KH, et al. Predicting response to multidrug regimens in cancer patients using cell line experiments and regularised regression models. *BMC Cancer.* 2015;15:235.
4. Mori S, Rempel RE, Chang JT, et al. Utilization of pathway signatures to reveal distinct types of B lymphoma in the Emicro-myc model and human diffuse large B-cell lymphoma. *Cancer Res.* 2008;68(20):8525-8534.
5. Metsalu T, Vilo J. ClustVis: a web tool for visualizing clustering of multivariate data using Principal Component Analysis and heatmap. *Nucleic Acids Res.* 2015;43(W1):W566-570.
6. Gerstner N, Kehl T, Lenhof K, et al. GeneTrail 3: advanced high-throughput enrichment analysis. *Nucleic Acids Res.* 2020;48(W1):W515-W520.
7. Liberzon A, Birger C, Thorvaldsdottir H, Ghandi M, Mesirov JP, Tamayo P. The Molecular Signatures Database (MSigDB) hallmark gene set collection. *Cell Syst.* 2015;1(6):417-425.
8. Yang S, Corbett SE, Koga Y, et al. Decontamination of ambient RNA in single-cell RNA-seq with DecontX. *Genome Biol.* 2020;21(1):57.
9. Stuart T, Butler A, Hoffman P, et al. Comprehensive Integration of Single-Cell Data. *Cell.* 2019;177(7):1888-1902 e1821.
10. Zhao J, Jaffe A, Li H, et al. Detection of differentially abundant cell subpopulations in scRNA-seq data. *Proc Natl Acad Sci U S A.* 2021;118(22)

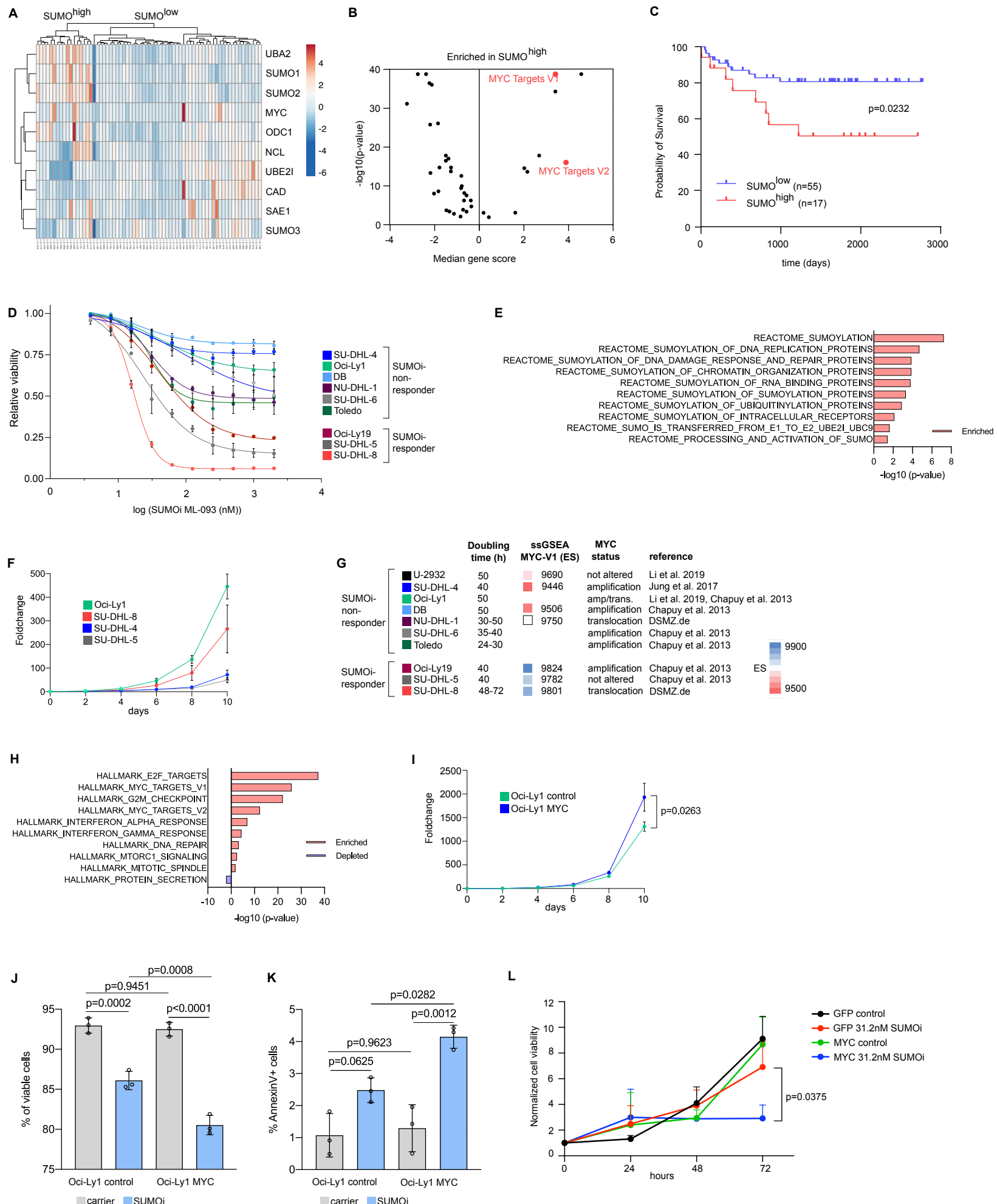
## SUPPLEMENTARY MATERIAL

### Antibodies

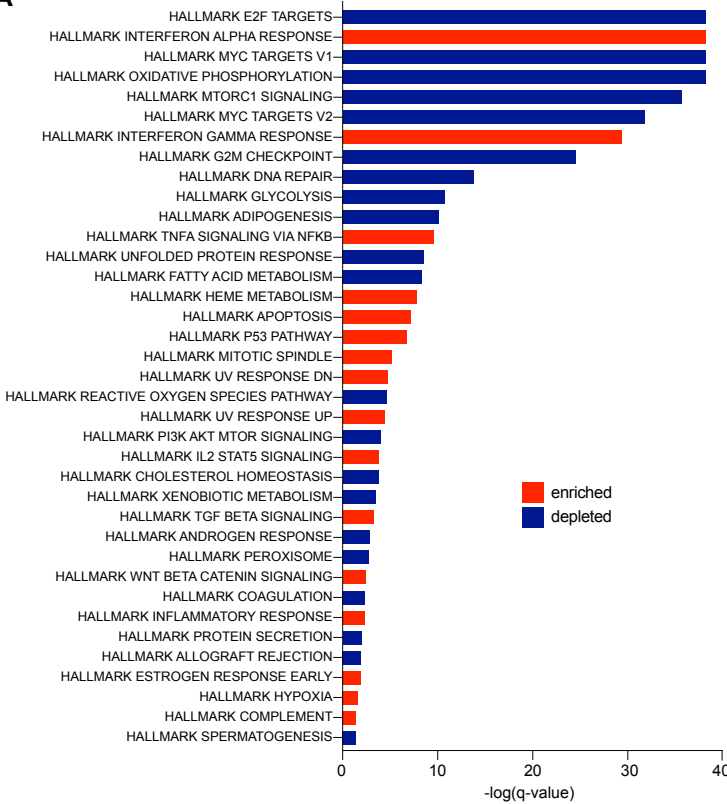
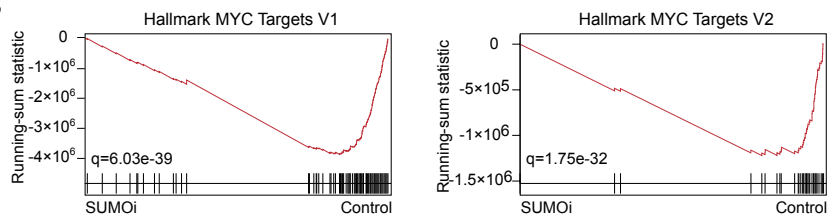
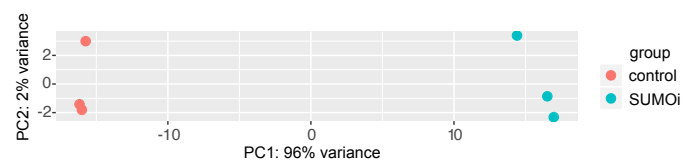
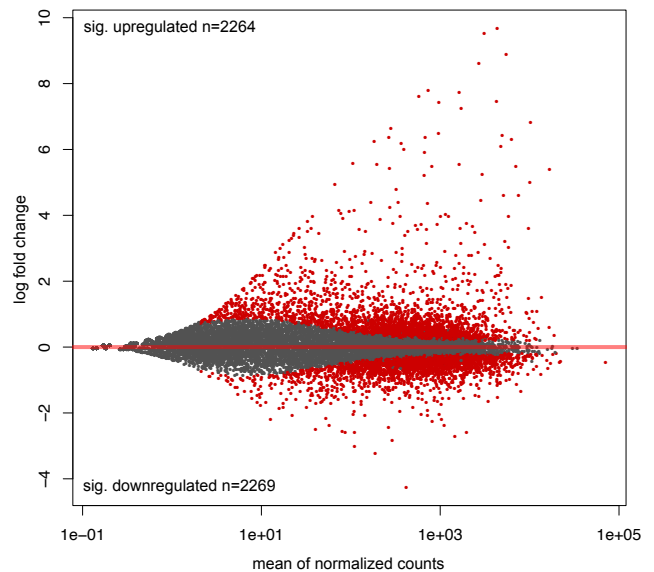
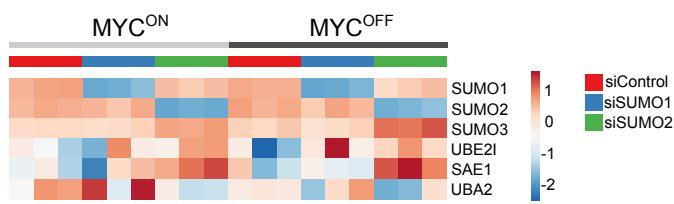
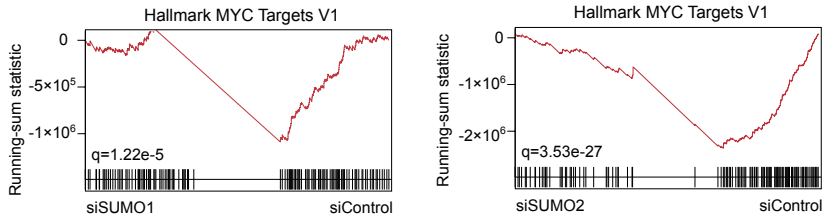
Epitope	Reactivity	Flurochrome	Company	Catalogue number
B220	mouse	PE-Cy7	Invitrogen	25-0452-82
B220	mouse	APC-Cy7	Invitrogen	47-0452-82
CD3e	mouse	PE-Cy5.5	Invitrogen	35-0031-82
CD4	mouse	PE-Cy7	Invitrogen	25-0041-82
CD8a	mouse	PE	BD	553032
CD19	mouse	eFluor450	eBioscience	48-0193-82
CD21/35	mouse	PE	BD	552957
CD23	mouse	PE-Cy7	Invitrogen	25-0232-82
CD25	mouse	FITC	Invitrogen	56-0251-82
CD44	mouse	FITC	Invitrogen	11-0441-82
CD62L	mouse	eFluor450	Invitrogen	48-0621-82
CD69	mouse	eFluor450	Invitrogen	48-0691-82
CD80	mouse	PE	eBioscience	12-0801-81
CD86	mouse	PE-Cy5/PerCP	Invitrogen	15-0862-81
CD127	mouse	APC	Invitrogen	17-1271-82
Foxp3	mouse	PE	eBioscience	12-5773-82
IgD	mouse	eFluor450	Invitrogen	48-5993-82
IgM	mouse	APC	Invitrogen	15-5790-82
MHC-II	mouse	APC-Cy7	eBioscience	47-5321-82
DAPI	all	-	Biolegend	422801
PI Solution	all	-	Sigma	25535-16-4

### Westernblot Antibodies

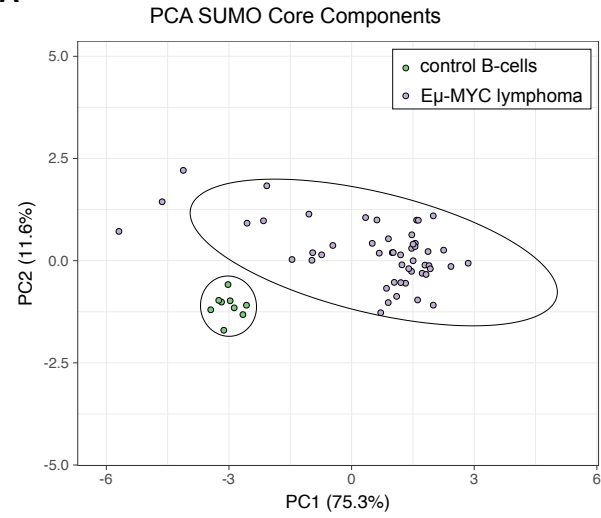
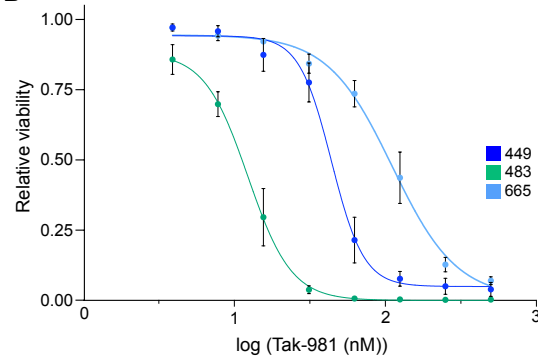
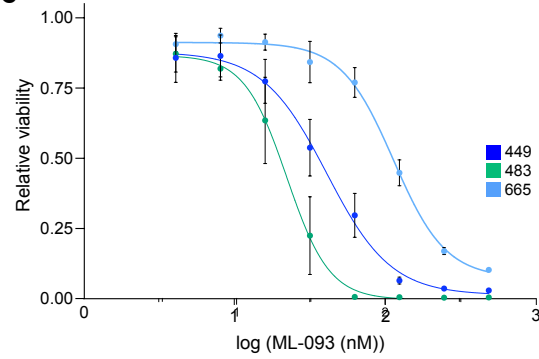
Target	Company	Article number
MYC	Cell signaling	9402S
$\beta$ -Tubulin	DSHB	E7



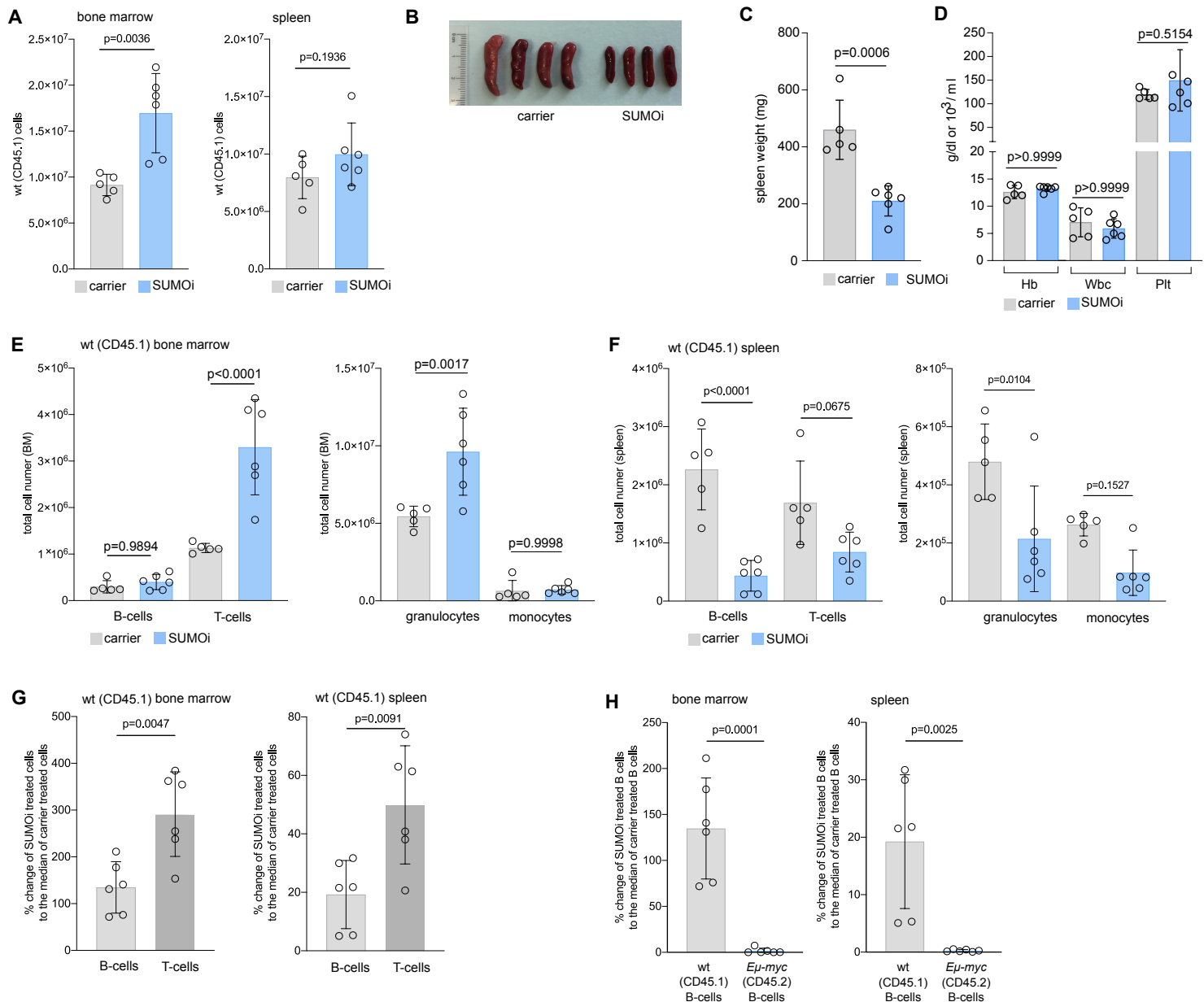
Supplementary Figure S1

**A****B****C****D****E****F**

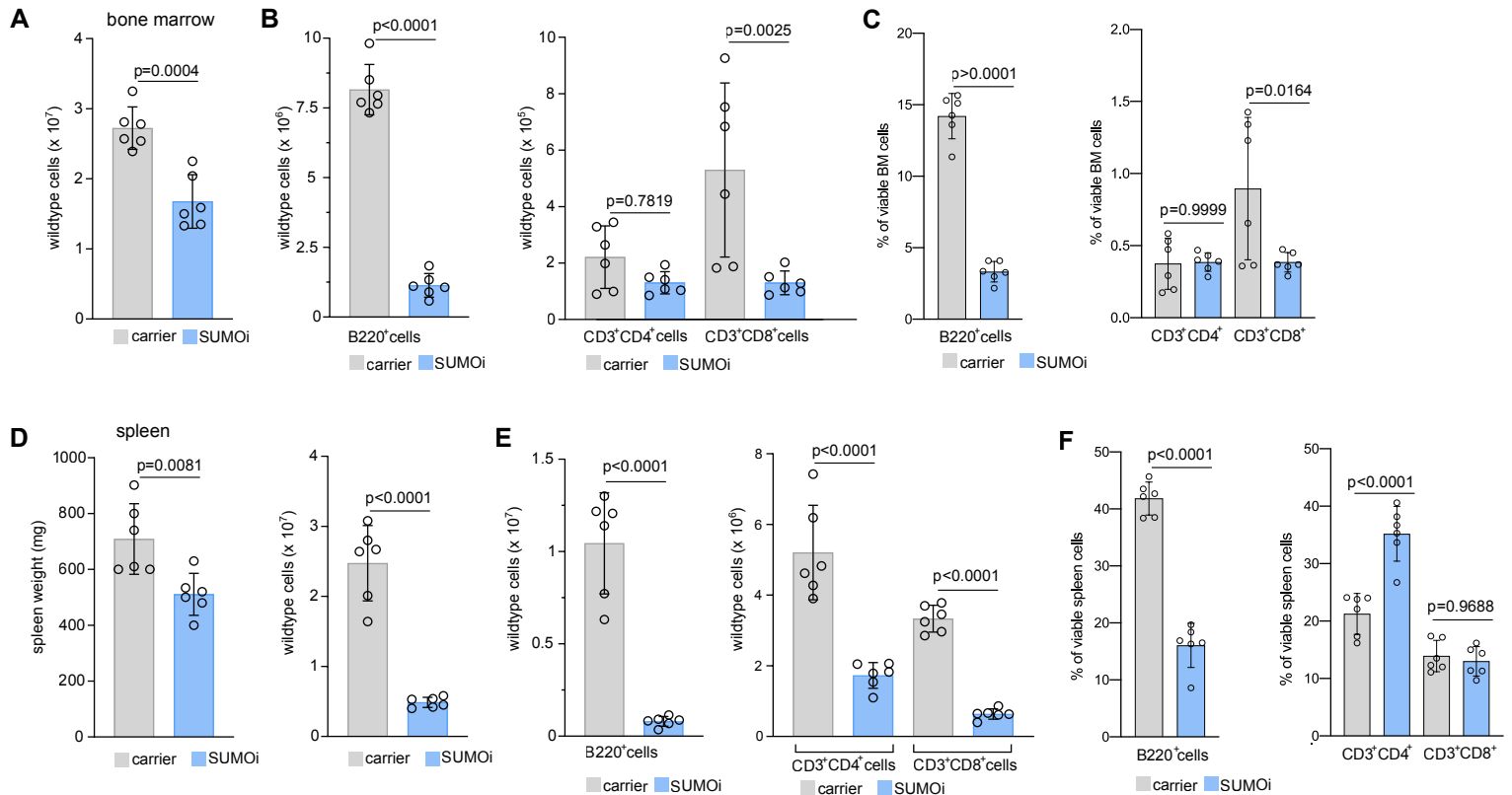
## Supplementary Figure S2

**A****B****C**

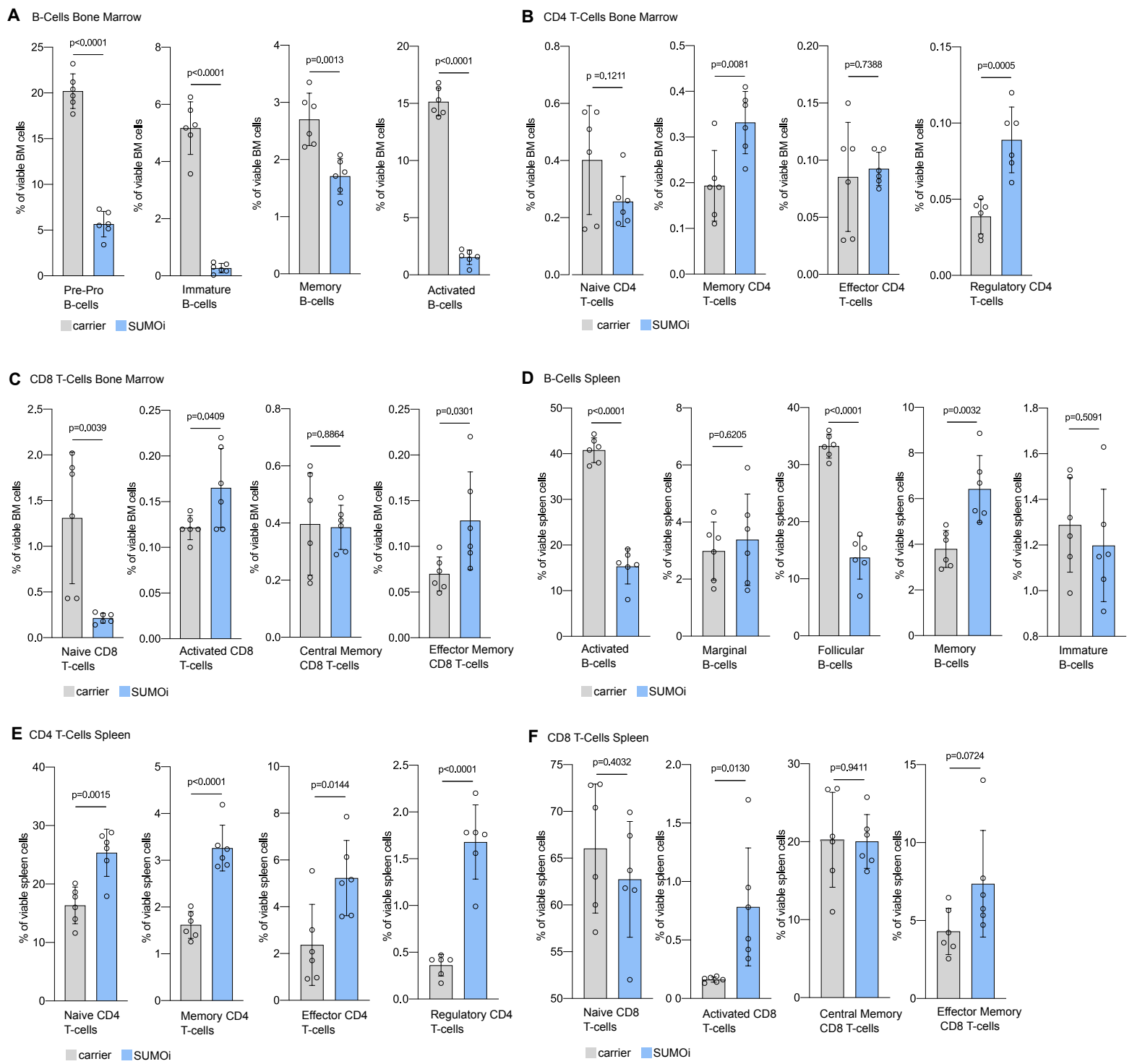
**Supplementary Figure S3**



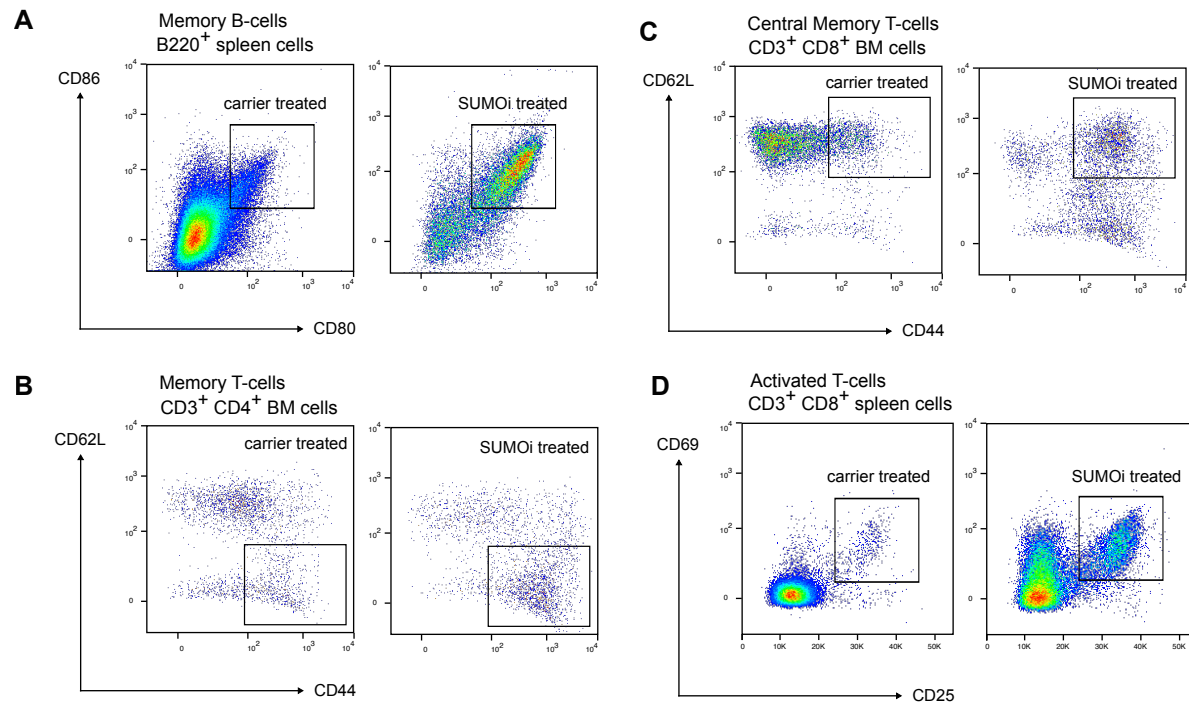
**Supplementary Figure S4**



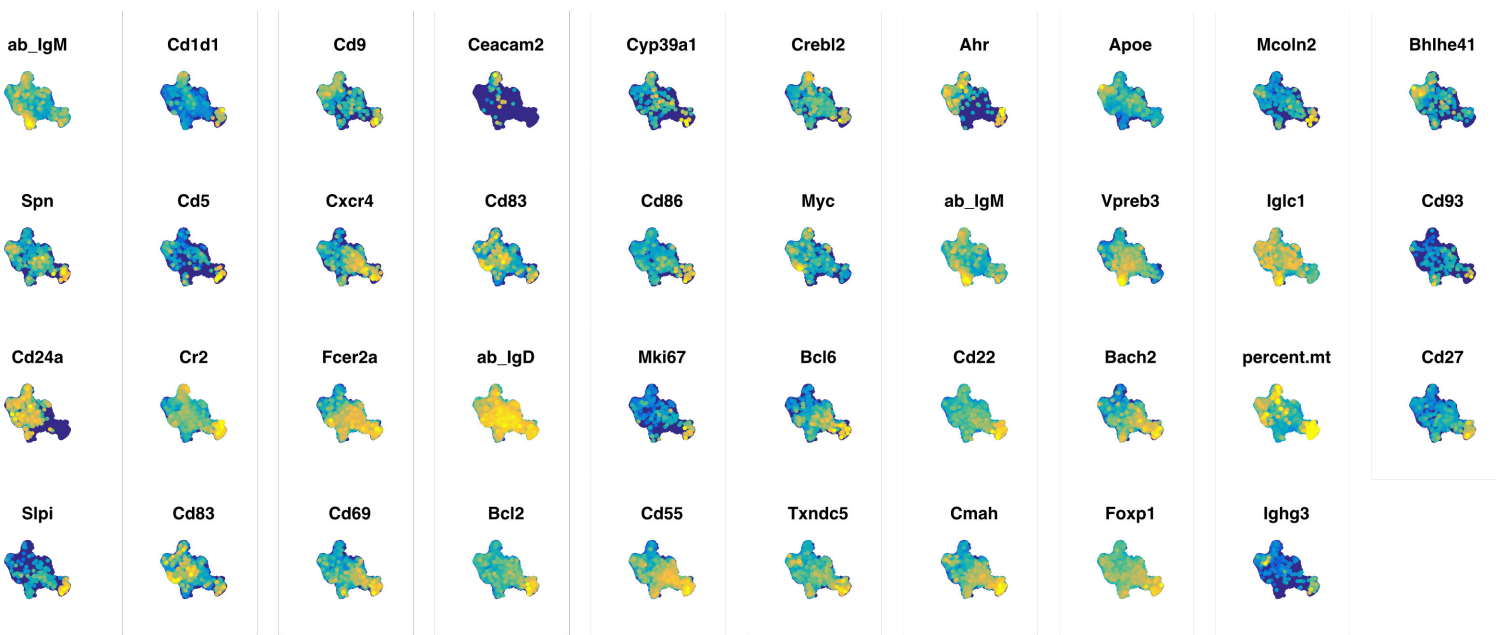
**Supplementary Figure S5**



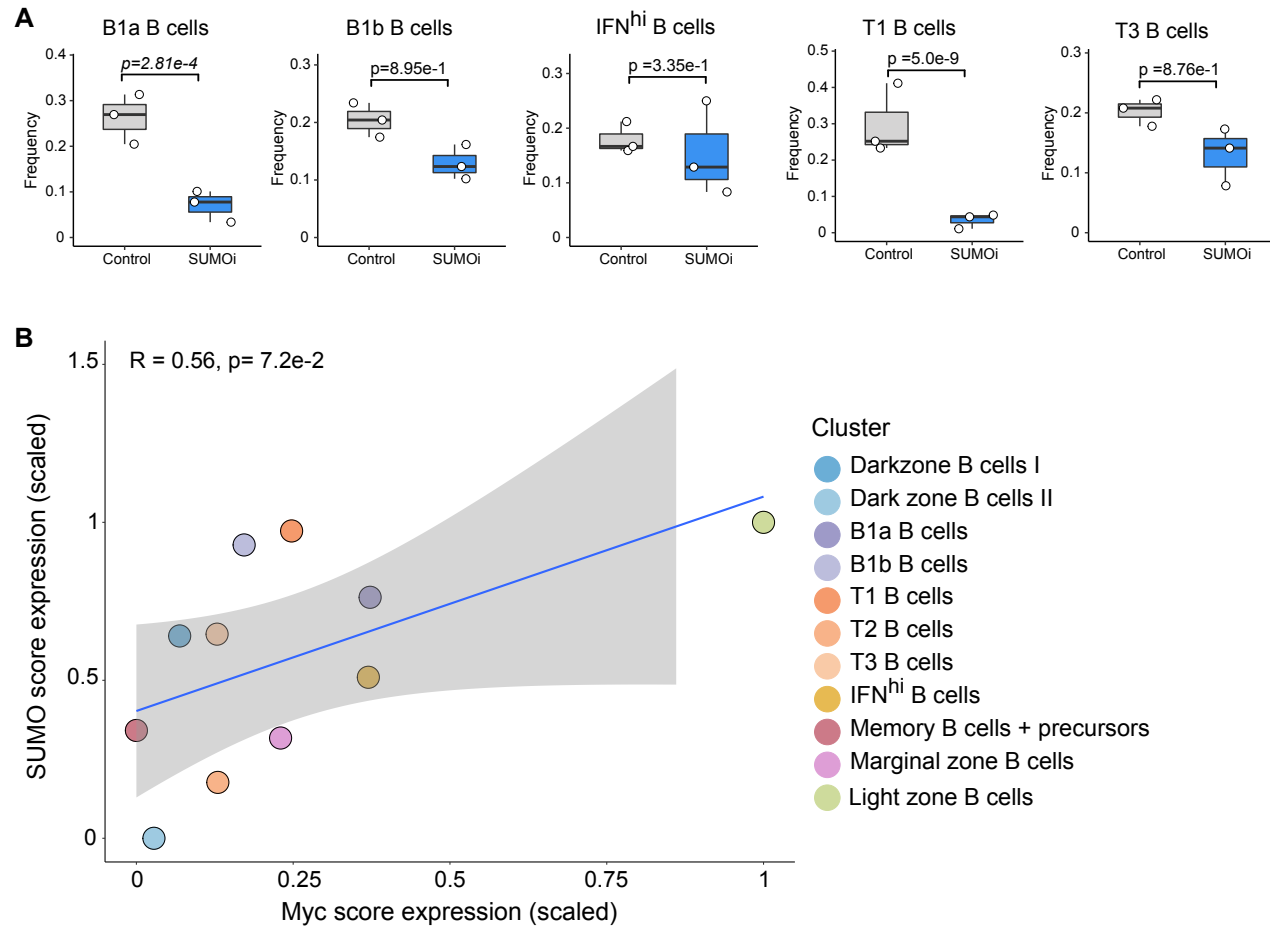
**Supplementary Figure S6**



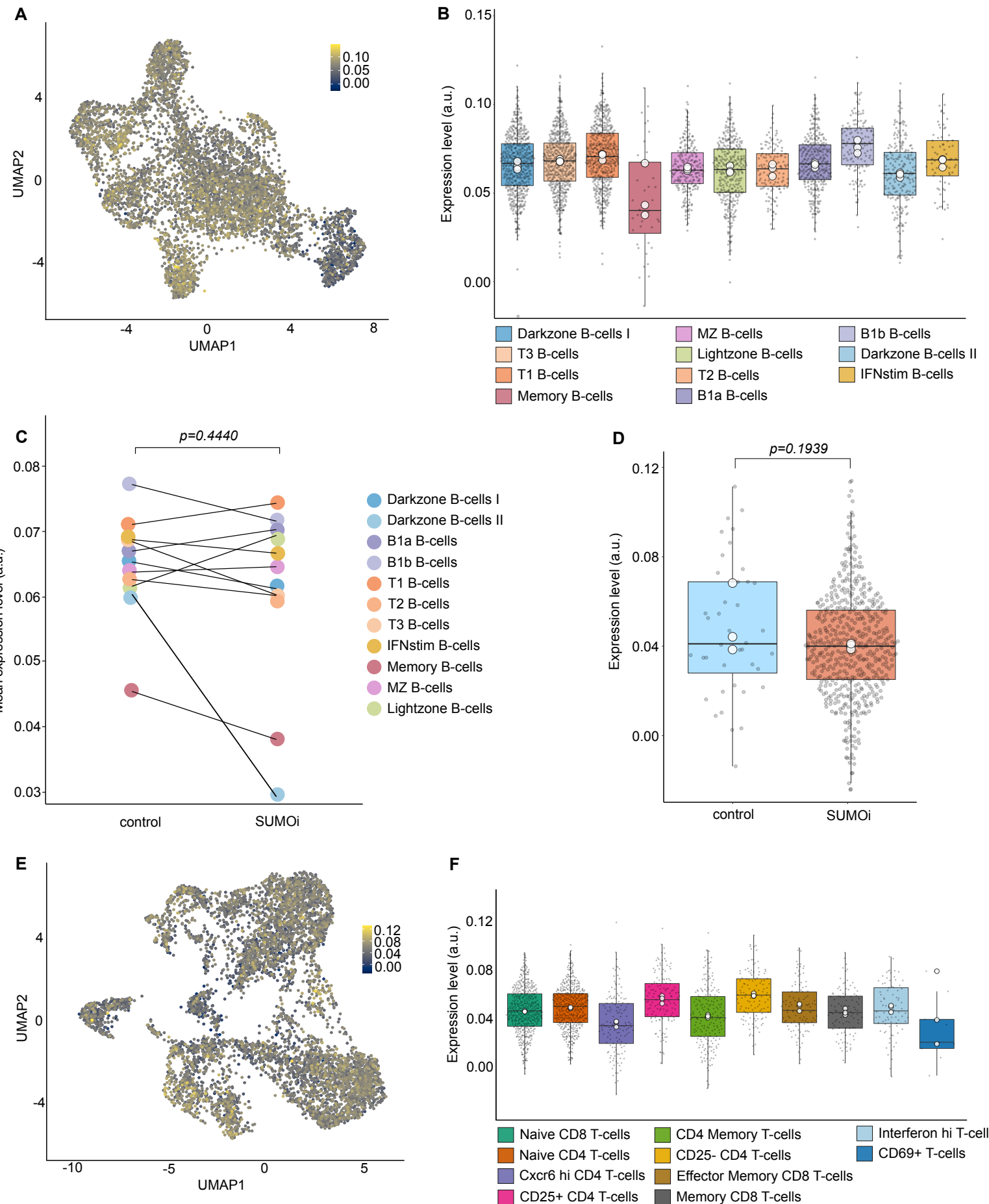
**Supplementary Figure S7**



**Supplementary Figure S8**



**Supplementary Figure S9**



Supplementary Figure S10

## SUPPLEMENTARY FIGURE LEGENDS

### Supplementary Figure S1.

- A) Hierarchical clustering (Euclidean/Ward) of indicated SUMO core components, MYC, and MYC target genes of normalized human DLBCL transcriptome profiles (GSE34171) revealed SUMO<sup>high</sup> and SUMO<sup>low</sup> subgroups as indicated.
- B) Gene set enrichment analysis of SUMO<sup>high</sup> and SUMO<sup>low</sup> subgroups identified in (A). Volcano plot displays significant gene signatures of the Hallmark gene set (MSigDb) with both MYC Hallmark signatures (v1, v2) highlighted.
- C) Kaplan-Meier-Plot of DLBCL patients from the GSE34171 dataset. Patient survival has been dichotomized based on the clustering method displayed in (A). Log rank p-value is indicated.
- D) Flow cytometry analysis of relative viability of indicated DLBCL cell lines treated with increasing SUMO $i$  concentrations (ML-093, 0, 3.9, 7.8, 15.6, 31.2, 62.5, 125, 250, 500, 1000, 2000nM) for 72h (n=3).
- E) Gene set enrichment analysis of SUMO $i$ -responder (Oci-Ly19, SU-DHL-5, SU-DHL-8) vs. SUMO $i$ -non-responder (U-2932, SU-DHL-4, DB, NU-DHL-1) on expression profiles accessed via GSE53798. Bar plot of enriched SUMOylation signatures, obtained from Reactome knowledgebase.
- F) Analysis of cell proliferation of two SUMO $i$  non-responder cell lines and two SUMO $i$ -responder cell lines.
- G) Table displaying doubling-time, MYC status and ssGSEA MYC-V1 enrichment score of each cell line. ssGSEA enrichment score representing the expression of genes in the MYC-V1 data set.
- H) Bar plot displaying top 10 enriched/depleted gene signatures of the Hallmark gene set (MSigDb) within SUMO $i$ -responding and SUMO $i$ -non-responding cells as described in (D).
- I) Analysis of cell proliferation of Oci-Ly1 cells transduced with a MYC expression plasmid or a control plasmid. P-value refers to cell proliferation on day 10 and is determined by unpaired t-test.
- J) Flow cytometric analysis of cell death of Oci-Ly1 cells transduced with a MYC expression plasmid or control plasmid, treated with control or SUMO $i$  (Tak-981, 31.2nM, 72h, n=3)
- K) Flow cytometric analysis of apoptosis of Oci-Ly1 cells transduced with a MYC expression plasmid or control plasmid, treated with control or SUMO $i$  (Tak-981, 31.2nM, 72h, n=3).
- L) Oci-Ly1 cells transduced with MYC plasmid or control plasmid were treated with SUMO $i$  (Tak-981, 31.2nM) and cell viability was measured by CellTiterGlo after 0, 24, 48 and 72h (n=3).

### Supplementary Figure S2.

- A) Summary of GSEA of expression data derived from transcriptome profiling Oci-Ly1 cells treated with control or SUMO $i$  (400nM, 48h) with the indicated gene sets. P-value determined by Kolmogorov-Smirnov test.
- B) Transcriptome analysis of RNAseq data from Oci-Ly1 cells, treated with the SUMO $i$  Tak-981 (400nM, 48h) revealed significant negative enrichments for both MYC hallmark gene sets. FDR-q values are indicated.

- C) Principal Component Analysis (PCA) of transcriptome profiles of Oci-Ly1 cells, treated with control or SUMO $\text{i}$  (400nM, 48h).
- D) MA plot visualizing differentially expressed genes (DEG) and their average expression. Significant genes were defined as all genes with an adj.p-value < 0.05. Here, n=2264 could be determined as significantly upregulated and n=2269 as significantly downregulated.
- E) U2OS-MYC<sup>tetON</sup> cells were seeded and simultaneously transfected with SUMO1, SUMO2 and control siRNAs. 42h after transfection cells were treated with either doxycyclin (MYC<sup>on</sup>) or a vehicle control (MYC<sup>off</sup>). After a total of 72h cells were harvested, RNA was isolated and analyzed by RNAseq. Heatmap indicates normalized mRNA expression levels of the SUMO core components SUMO1, SUMO2, SUMO3, SAE1, UBA2 and UBE2I.
- F) Enrichment plots of Hallmark MYC targets V1 indicating significant negative enrichments in U2OS-MYC<sup>on</sup> SUMO1 or SUMO2 knockdown cells (as described in Fig.S2E). FDR-q values are indicated.

#### **Supplementary Figure S3.**

- A) Transcriptome data from murine *Eμ-Myc* induced lymphomas and healthy B-cells was accessed via GSE7897. The SUMO core machinery components Sumo1, Sumo2, Sumo3, Ube2i, Uba2, Sae1 have been used for principal component analysis (PCA).
- B) Flow cytometry analysis of relative viability of indicated murine *Eμ-Myc* lymphoma cell lines treated with increasing SUMO $\text{i}$  concentrations (0, 3.9, 7.8, 15.6, 31.2, 62.5, 125, 250, 500, 1000, 2000nM) for 72h (n=3) using Tak-981.
- C) Flow cytometry analysis of relative viability of indicated murine *Eμ-Myc* lymphoma cell lines treated with increasing SUMO $\text{i}$  concentrations (0, 3.9, 7.8, 15.6, 31.2, 62.5, 125, 250, 500, 1000, 2000nM) for 72h (n=3) using ML-093.

#### **Supplementary Figure S4.**

- A) Total number of wild-type (wt, CD45.1) cells in the bone marrow (BM) and spleen after carrier vs. SUMO $\text{i}$  treatment (ML-093, 50mg/kg). N=6, p-values was determined by unpaired t-test.
- B) Picture of representative spleens of *Eμ-myc* lymphoma mice after carrier vs. SUMO $\text{i}$  treatment (treatment scheme outlined in Fig. 2A).
- C) Spleen weight following SUMO $\text{i}$  treatment. N=6, p-value was determined by unpaired t-test.
- D) Analysis of hemoglobin (Hb), white blood cells (Wbc) and platelets (Plt) after carrier vs. SUMO $\text{i}$  treatment. P-values were determined by ANOVA; Tukey's post hoc test.
- E) Total number of wt (CD45.1) B-cells (B220 $^+$ ), T-cells (CD3 $^+$ ), granulocytes (Gr. 1 $^+CD11b^+$ ) and monocytes (Gr.1 $^+CD11b^+$ ) in the BM following SUMO $\text{i}$  treatment compared to carrier. N=6, P-values were determined by ANOVA; Tukey's post hoc test.
- F) Total number of wt (CD45.1) B-cells (B220 $^+$ ), T-cells (CD3 $^+$ ), granulocytes (Gr. 1 $^+CD11b^+$ ) and monocytes (Gr.1 $^+CD11b^+$ ) in the spleen following SUMO $\text{i}$  treatment compared to carrier. N=6, P-values were determined by ANOVA; Tukey's post hoc test.
- G) Relative change of SUMO $\text{i}$ -treated B-cells and T-cells cells to the median number of the respective carrier-treated cell population in BM and spleen. N=6, p-values was determined by unpaired t-test.

- H) Relative change of SUMO $\text{i}$ -treated B-cells to the median number of carrier-treated B-cells, calculated for wt and E $\mu$ -myc B-cells in BM and spleen. N=6, p-values were determined by unpaired t-test.

**Supplementary Figure S5.**

- A) Total number of BM cells after carrier vs. SUMO $\text{i}$  treatment, as outlined in Fig. 3A. N=6, p-value was determined by unpaired t-test.
- B) Total number of indicated cell populations (B220+ B-cells, CD3+CD4+ T-cells, CD3+CD8+ T-cells) in the BM after carrier vs. SUMO $\text{i}$  treatment. N=6, p-values were determined by unpaired t-test.
- C) Relative number of indicated cell populations (B220+ B-cells, CD3+CD4+ T-cells, CD3+CD8+ T-cells) of viable BM cells after carrier vs. SUMO $\text{i}$  treatment. N=6, p-values were determined by unpaired t-test.
- D) Spleen weight and total number of spleen cells after carrier vs. SUMO $\text{i}$  treatment for 48h. N=6, p-values were determined by unpaired t-test.
- E) Total number of indicated cell populations (B220+ B-cells, CD3+CD4+ T-cells, CD3+CD8+ T-cells) in the spleen after carrier vs. SUMO $\text{i}$  treatment. N=6, p-values were determined by unpaired t-test.  
Relative number of indicated cell populations (B220+ B-cells, CD3+CD4+ T-cells, CD3+CD8+ T-cells) of viable spleen cells after carrier vs. SUMO $\text{i}$  treatment. N=6, p-values were determined by unpaired t-test.

**Supplementary Figure S6.**

- A) Relative number of indicated B220+ BM cell populations (B220+IgM- Pre-Pro B-cells, B220+IgM+IgD- Immature B-cells, B220+CD80+CD86+ Memory B-cells, B220+CD19+MHC-II+ Activated B-cells) of viable BM cells after carrier vs. SUMO $\text{i}$  treatment. N=6, p-values were determined by unpaired t-test.
- B) Relative number of indicated CD3+CD4+ BM cell populations (CD3+CD4+CD44lowCD62L+ Naïve T-cells, CD3+CD4+CD44highCD62L- Memory T-Cells, CD3+CD4+CD44lowCD62L- Effector T-cells, CD3+CD4+CD25+CD69+FoxP3+ Regulatory T-cells) of viable BM cells after carrier vs. SUMO $\text{i}$  treatment. N=6, p-values were determined by unpaired t-test.
- C) Relative number of indicated CD3+CD8+ BM cell populations (CD3+CD8+CD44lowCD62L+ Naïve T-cells, CD3+CD8+ CD44highCD62L- Effector Memory T- Cells, CD3+CD8+CD44highCD62L+ Central Memory T-cells, CD3+CD8+CD25+CD69+ Activated T-cells) of viable BM cells after carrier vs. SUMO $\text{i}$  treatment. N=6, p-values were determined by unpaired t-test.
- D) Relative number of indicated B220+ spleen cell populations (B220+CD93+ Immature B-cells, B220+CD21highCD23low Marginal zone B-cells, B220+CD21lowCD23high Follicular B-cells, B220+CD80+CD86+ Memory B-cells, B220+CD19+MHC-II+ Activated B-cells) of viable spleen cells after carrier vs. SUMO $\text{i}$  treatment. N=6, p-values were determined by unpaired t-test.
- E) Relative number of indicated CD3+CD4+ spleen cell populations (CD3+CD4+CD44lowCD62L+ Naïve T-cells, CD3+CD4+CD44highCD62L- Memory T-Cells, CD3+CD4+CD44lowCD62L- Effector T-cells, CD3+CD4+CD25+CD69+FoxP3+ Regulatory T-cells) of viable spleen cells after carrier vs. SUMO $\text{i}$  treatment. N=6, p-values were determined by unpaired t-test.
- F) Relative number of indicated CD3+CD8+ spleen cell populations (CD3+CD8+CD44lowCD62L+ Naïve T-cells, CD3+CD8+CD44highCD62L- Effector

Memory T-Cells, CD3+CD8+ CD44highCD62L+ Central Memory T-cells, CD3+CD8+CD25+CD69+ Activated T-cells) of viable spleen cells after carrier vs. SUMO<sub>i</sub> treatment. N=6, p-values were determined by unpaired t-test.

#### **Supplementary Figure S7.**

- A) Scheme indicating gating strategy for Memory B-cells ( $B220^+CD80^+CD86^+$ ) in the spleen after carrier vs. SUMO<sub>i</sub> treatment, as indicated in Fig. 3A.
- B) Representative FACS plots illustrating gating strategy for Memory T-cells ( $CD3^+CD4^+CD44^{high}CD62L^-$ ) in the BM after carrier vs. SUMO<sub>i</sub> treatment.
- C) Scheme indicating gating strategy for  $CD3^+CD8^+$  Central Memory T-cells ( $CD3^+CD8^+CD44^{high}CD62L^+$ ) in the BM after carrier vs. SUMO<sub>i</sub> treatment.
- D) Representative FACS plots illustrating gating strategy for Activated T-cells ( $CD3^+CD8^+CD25^+CD69^+$ ) in the spleen after carrier vs. SUMO<sub>i</sub> treatment.

#### **Supplementary Figure S8.**

- A) Featureplots of B cell marker genes that were used to annotate the B cell populations. Yellow = high expression; Blue = low expression

#### **Supplementary Figure S9.**

- A) Differential abundance analysis on mouse-wise pseudobulks (indicated by white dots, n=3). Bar plots represent the subpopulation frequencies stratified by condition. The median is indicated by the center line of the box plot. The box extends from the 25<sup>th</sup> to 75<sup>th</sup> percentiles, whisker length reaches from minimum to maximum. Significance is determined by a Negative Binomial Generalized Linear Model.
- B) SUMO and MYC score correlation analysis in SUMO<sub>i</sub> treated mice. Scaled mean expression values are plotted against each other for each subpopulation identified in Fig. 5B. R indicates the Pearson correlation coefficient. The regression line is shown in blue. The grey area indicates the 95% confidence interval.

#### **Supplementary Figure S10.**

- A) UMAP of control and SUMO<sub>i</sub> treated B cells with highlighted expression of the proliferation module score.
- B) Expression level of the proliferation score in control B cell subsets. Grey dots represent the individual cells. The back line indicates the median across all cells. White dots represent the median score expression per mouse-wise pseudobulk.
- C) Pairwise comparison of the mean proliferation score expression in B cell populations. Significance was tested using a paired t-test.
- D) Expression level of the proliferation score in memory B-cells. A two-sided Wilcoxon rank sum test was applied to determine significance. Grey dots indicate the individual cells. The back line represents the median across all cells. White dots indicate the median score expression per mouse-wise pseudobulk.
- E) UMAP of control and SUMO<sub>i</sub> treated T cells with highlighted expression of the proliferation module score.
- F) Expression level of the proliferation score in control T cell subsets. Grey dots represent the individual cells. The back line indicates the median across all cells. White dots represent the median score expression per mouse-wise pseudobulk.